Review 1

This work showed that the eddy viscosity component is still dominant even when stratification is present. Particularly, the turbulent mean component dominates the overall eddy viscosity component under stratified conditions. In contrast, under unstratified conditions, the contribution of the tidal straining component to the total eddy viscosity component outweighs that of other components. The authors presented a lot of figures in their work to show the results and findings (i.e., 17 figures in total). However, the authors are encouraged to more selective with the figures. The authors did a good job in presenting interesting experiments and results to the scientific community. However, as there are a few things requiring improvement in the manuscript at this point, it is suggested that the article should go through minor revisions and English editing before accepting and publishing. Specific review comments are provided to the authors as follows.

Response: We would like to thank you for your careful reading, helpful comments, and constructive suggestions, which have significantly improved the presentation of our manuscript. We appreciate all your professional comments and have revised our manuscript accordingly. The original 17 figures have been consolidated into 13, and Table 2 has been transformed into a bar chart, bringing the total number of figures to 14 in the revised manuscript (figures appended at the end). Additionally, we have made further revisions and refined the English based on the reviewer's suggestions.

Lines 059 – 059: It should be "gravitational circulation" instead of "gravity circulation".

Response: The "gravity circulation" has been changed into "gravitational circulation" (line 59).

Lines 061 – 062: It is understood that the authors already provided brief comparison in lines 086 – 090. However, the authors are encouraged to provide a brief introduction and definition of ERV and LRV when they first appeared in the paper. For example, one of the authors' previous works published on the Frontiers in Marine Science (Deng et al., 2022; https://doi.org/10.3389/fmars.2022.901490) mentioned that "Eulerian residual velocity (ERV) is the average of the velocities during one or several tidal periods at a fixed location (Abbott, 1960). Lagrangian residual velocity (LRV) is defined as the net displacement of a labeled water parcel over one or several tidal periods (Zimmerman, 1979)."

Response: In the revised manuscript, concise definitions of ERV (lines 61–63) and LRV (lines 103–105) have been included at their initial mentions in the paper. "*To remove the tidal signal, early researchers such as Abbott (1960) utilized a straightforward method by averaging current velocities over one or several tidal periods at a specific location to calculate the Eulerian Residual Velocity (ERV).*" "*Zimmerman (1979) defined Lagrangian residual velocity (LRV) as the net displacement of the water parcels*

over one or several tidal periods."

Lines 077 – 085: While several relevant works have been reviewed and included, the authors are encouraged to include some most-recent studies. For example, Hewageegana et al. (2023; https://doi.org/10.3390/jmse11071333) used a numerical model (ROMS) to analyze the seasonal variation of residence time at Caloosahatchee River Estuary, Florida during a period of five years. Hewageegana et al. (2023) discovered and showed a relationship between residence time and wind direction and magnitude.

Response: The most recent studies have been induced in the revised manuscript (lines 80–90; lines 96–99; lines 108–122; lines 160–162). "*Wind, in conjunction with tides and density gradients, exerts a substantial influence on estuarine residual currents and stratification (Verspecht et al., 2009; Jongbloed et al., 2022). Its role in the generation of surface residual currents is underscored by the strong correlations observed between wind speeds and residual current velocities across both annual and seasonal timescales (Ren et al., 2022). Research on the Dongsha atoll revealed that the combined effects of wind and tide introduce more dynamic water exchange compared to tides alone (Chen, 2023). In the Bohai Sea area off Qinhuangdao, residual currents exhibit pronounced seasonal fluctuations, correlating notably with wind speeds at specific temporal lags (Zhang et al., 2023). Furthermore, the shift in wind-driven circulation is pivotal for mass transport within bays, with estuarine residual circulation superseding tidal pumping as the primary transport mechanism (Young et al., 2023).*"

"*Wind plays a pivotal role in modulating classical gravitational circulation, most notably reversing surface outflow during winter. In contrast, northward winds in spring enhance stratification and augment the pressure gradient-driven flow (Soto-Riquelme et al., 2023).*"

"*Lagrangian particle tracking methods play a pivotal role in studying mass transport and residence time (RT) across various coastal seas, estuaries, and bays. Specific water mass transport patterns are discerned in the Bohai Sea, revealing salient regional transport characteristics steered by LRV (Yu et al., 2023). The combined effects of residual transport velocity in the current and next seasons emerge as the predominant factor driving the RT's seasonal variation (Lin et al, 2022). Wind direction, wind speed, and density gradient-induced circulation collectively regulate RT (Hewageegana et al., 2023). The reduction of cross-shore currents results in mass convergence and increases RT (Li et al., 2022). The water exchange and RT are mainly determined by the structure of the LRV (Jiang and Feng, 2014). RT predominantly represents an accumulative measure, primarily influenced by residual transport rather than immediate responses (Jiang, 2023). Convergence zones resulting from LRV efficiently establish consistent aggregation regions of buoyant material within the estuary rather than ERV (Kukulka and Chant, 2023). To gain an in-depth understanding*

of mass transport, extensive prior research has been dedicated to elucidating qualitative and quantitative evaluations of the determinants impacting the LRV's structure and magnitude."

"*An anticlockwise shift in summertime wind direction from 1979 to 2020 weakens cross-channel wind-driven transport and along-channel seaward flow, leading to increased stratification near the Modaomen (Hong et al. 2022).*"

Lines 177 – 178: It is recommended to write it as either "tidal periodic oscillation currents" or "periodic oscillation tidal currents". In other words, use one "tidal" instead of two.

Response: The "tidal periodic oscillation tidal currents" has changed into "tidal periodic oscillation currents" (lines 210–211).

Lines 195 – 206: The authors indicated the model setup in detail in this section. However, the authors are encouraged to indicate more about how the resolution in space and time were determined. For example, did the model setup follow some previous studies? (If yes, please include the reference.) Or did the authors perform a sensitivity analysis on computational grid resolution for this work?

Response: Yes, the resolutions in space and time for model setup are based on previous studies. The references are added to the revised manuscript (lines 247–249). "*On the other hand, the fine grid, consisting of 45,368 nodes and 87,179 triangular elements, is configured based on the settings from previous studies. (e.g., Lai et al., 2018; Geyer et al., 2020; Xu et al., 2021).*" For instance, Geyer et al. (2020) employed an average grid spacing of 100 meters in the cross-estuary direction and 165 meters in the along-estuary direction while investigating exchange flow mechanisms in Delaware Bay. Xu et al. (2021) used resolutions ranging from 100 in the inlets to 3000 meters along the coastal ocean when exploring the nonlinearity of residual currents in the Pearl River estuary (PRE). Lai et al. (2018) utilized resolutions varying from 0.1 to 10 kilometers across the entire domain: 0.1–0.3 kilometers inside the Pearl River Estuary, 0.3–0.5 kilometers at the estuary mouth, 1.0–2.0 kilometers in Guangdong coastal waters, and 10 kilometers near the open boundary to examine the impact of tides and winds on Eulerian residual velocity. Considering computational efficiency and drawing on insights from prior research in real estuaries and bays, the paper adopts specific grid resolutions. Specifically, fine grids with a resolution of 0.1 kilometers are utilized within the PRE, the primary focus area, as well as 0.1 to 1.0 kilometers off the Guangdong coast and 2.0 kilometers near the open boundary.

The temporal resolution must adhere to the Courant-Friedrichs-Lewy (CFL) condition when spatial resolutions are specified. In theory, considering the spatial resolution and water depth in the PRE, the CFL value should ideally be less than 4 seconds. However, in practice, an external time step of 0.5 seconds is chosen to maintain model stability, especially when dealing with triangular grids and intricate

topography and coastlines. Additionally, a split number of 10 is applied under these conditions when a split-mode time-stepping method is used.

Lines 210 – 215: The authors are encouraged to indicate both references and links. The authors are also encouraged to indicate the time interval (i.e., resolution in time) of the CCMP data. Additionally, the authors are encouraged to indicate the full name of "CCMP" as it appeared in the document for the first time.

Response: In the revised manuscript, we have provided the references and links for these datasets, specified the time interval for the CCMP data, and included the full name of CCMP (lines 256–274). "*The model incorporates eight major tidal constituents, namely M_2, N_2, S_2, K_2, K_1, O_1, P_1, and Q_1, as tidal driving forces at the open boundary. These constituents are obtained from the Oregon State University Tidal Prediction Software (OTPS/TPXO; https://www.tpxo.net/otps; Egbert and Svetlana, 2002). To initialize the model, salinity climatological data from the 1° World Ocean Atlas 2009 (WOA2009) dataset is utilized (https://accession.nodc.noaa.gov/0094866; Levitus, 2013). The wind data used in this study are obtained from the monthly averaged Cross-Calibrated Multi-Platform (CCMP) dataset, which has spatial resolutions of 0.25×0.25 degrees (http://www.remss.com/measurements/ccmp; Mears et al., 2022). The Pearl River Estuary (PRE) experiences seasonal reversing monsoonal winds, as documented by Pan et al. (2014) and Pan and Gu (2016). The monthly-averaged CCMP wind data indicate prevalent southwesterly winds during the summer season. Our investigation specifically focuses on the impact of southwesterly winds on the dynamics of Lagrangian Residual Velocity (LRV). The lateral boundary incorporates monthly average river runoff data from eight river inlets, which are provided by the Water Conservancy Committee of the Pearl River under the Ministry of Water Resources. The topography data off the PRE is from the ETOPO2 dataset of NOAA (https://www.ngdc.noaa.gov/mgg/global/relief/-ETOPO2/ETOPO2v2-2006/; NOAA National Geophysical Data Center, 2006), while the topography within the estuary is derived from electronic nautical chart data provided by the China Maritime Safety Administration.*"

Lines 223 – 223: The authors are encouraged to indicate the date, e.g., 1 June 2017.

Response: The specific dates have been included in the revised manuscript (line 278). "*The fine grid model, which begins on 1 June 2017*"

Lines 242 – 242: It should be "… including three cross sections (Sections B – D)".

Response: Yes, it should be "*The paper selects four sections, including three cross sections (Sections B–D)*" (lines 296–297).

Lines 245 – 249: According to the description in lines 241 – 244, should these along-estuary distributions of salinity be extracted from Section A instead of Section C? It may be clearer to move the texts in the subplots' titles "CTD" and "MODEL" to the space after "(b)" and "(c)" in the plots. In other words, the authors are encouraged to

revise “(b)” as “(b) CTD” and revise “(c)” as “(c) MODEL” on the plots. Additionally, although the authors have indicated that the colormap represents salinity in the figure caption, it may be clearer to indicate that beside the color bar as well.

Response: Along-estuary salinity distributions are sourced from CTD observation stations, with the station layout closely matching Section A. Associated captions have been updated accordingly (lines 306–307). “*(b) Along-estuary salinity profiles based on CTD depth-profiled data, closely aligned with Section A; (c) salinity outputs from the numerical model*.”

In the initial manuscript, lines 241–244 highlight that “*The examination of LRV components and the eddy viscosity subcomponent is presented solely in Section C, given the uniform conclusions derived across four sections. Moreover, the chosen cross-section, Section C, aptly depicts the differential dynamics of LRV between the shoal and the deep channel*”, which has been rephrased for clarity in the updated manuscript (lines 298–302)

In the revised manuscript, the titles "CTD" and "MODEL" in Figs. 2b and c have been updated to "(b) CTD" and "(c) Model", respectively. Additionally, the caption adjacent to the color bar has been changed from "(psu)" to "Salinity (psu)".

Lines 250 – 250: It may be clearer to revise the “model-derived elevation” as “model-derived sea surface elevation”.

Response: The term "model-derived elevation" has been modified to "model-derived sea surface elevation" (line 308). “*Model verification involves comparing the model-derived sea surface elevation……*”

Lines 267 – 267: It should be “good performance” instead of “well performance”.

Response: The term "well performance" has been revised to "good performance" (line 326).

Lines 268 – 268: It may be clearer to represent the y-label as “Sea surface elevation” instead of “Sea level”, which is also consistent with the description in line 252.

Response: The label on the y-axis in Figure 3 has been updated from "Sea level" to "Sea surface elevation."

Lines 275 – 275: It should be rewritten as “where abs is the absolute value function …”.

Response: The sentence “where abs are the absolute value function” has been modified to “where abs is the absolute value function” (line 334).

Lines 294 – 299: While panels (a) to (e) in Figure 4 have been introduced in the figure caption, panels (f) to (j) are NOT introduced. Additionally, although the authors have indicated that the colormap represented uL in the figure caption, it may be clearer to indicate that beside the color bar as well. This comment also applies to Figures 5 – 17.

Response: In Fig. 4, the panels in the right columns have been detailed in the figure captions, and the associated annotations adjacent to the color bar have been updated in the revised manuscript. Analogous modifications have been implemented in other

figures (Fig. 5–14) in the revised manuscript.

Lines 306 – 307: This comment is optional. The authors are encouraged to think about how to better present the data shown in Table 2 to the readers. Would it be more appropriate and clearer if these data/numbers are presented using bar charts or something similar?

Response: Table 2 has been substituted with bar charts.

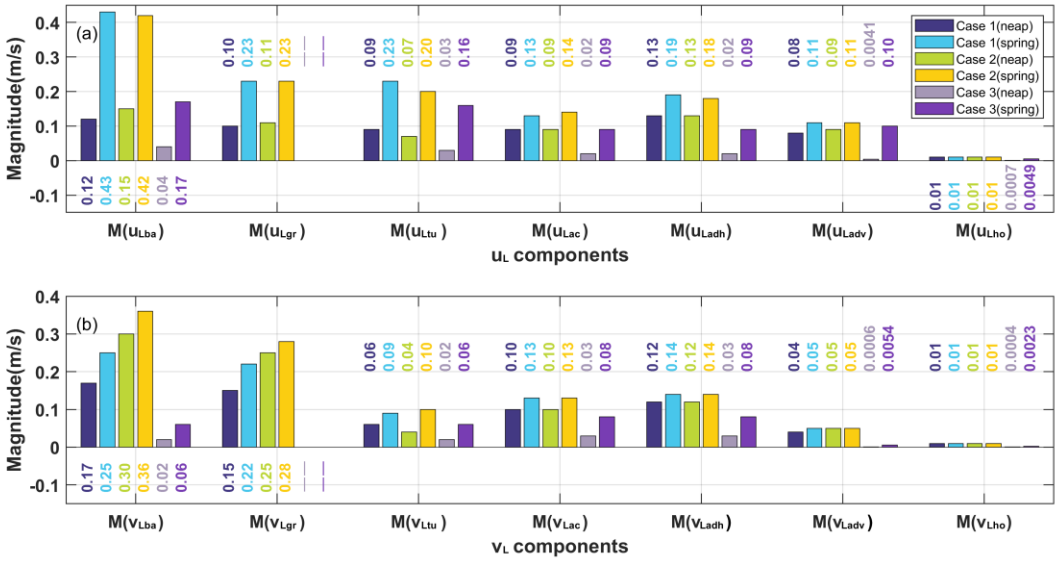

Figure 5 Bar charts for the magnitude of each component of u_L and v_L.

Lines 402 – 402: The authors are encouraged to use numbers to describe/rephrase "significant changes" or "there is no significant change" throughout the document e.g., lines 454, 489, 605, 646, 668, and 748).

Response: We have replaced the phrases "significant changes" and "there is no significant change" by quantitative values (lines 495–497; lines 531–534; lines 648–650; lines 684–687; lines 720–722; lines 746–749; lines 757–764; lines 822–823). "*with the exception of the noticeably reduced along-estuary eddy viscosity component (v_{Ltu}) by one order of magnitude in the upper layer in Case 2 during neap tides (Fig. 9g) and slightly intensified during spring tides (Fig. 9n) compared to scenarios with wind.*" "*the findings indicate that the cross-estuary eddy viscosity component modulates the configuration of the cross-estuary LRV. In the upper layers, this component exhibits an enhancement of an order of magnitude under the influence of the dominant southwesterly winds, relative to conditions in the absence of wind in the PRE.*" "*However, during neap tides, their magnitudes in the upper layer manifest a reduction by an order of magnitude relative to Case 1. This indicates a substantial influence of wind on these subcomponents during relatively small tides.*" "*The results elucidate the substantial effect of stratification on each non-dominant component of the eddy viscosity due to the differentially sheared structure, with magnitudes an order greater*

than in non-stratified scenarios." "*The results in the paper have indicated that the contribution of the horizontal diffusion component is several-fold lower, or even an order of magnitude less, than other components*." "*The findings underscore that the southwesterly wind amplifies the relative contribution ratios of the tidal straining component to the baroclinic pressure gradient component of the LRV. Specifically, these ratios are 1.5 to 3 times greater compared to scenarios without wind forcing.*" "*This paper reveals that under stratified conditions, the tidal mean component dominates the eddy viscosity, even though the magnitudes of tidal straining and the combined component of tidal-average eddy viscosity and velocity gradient oscillation are greater than the turbulent mean component. However, these two components exhibit inverse structures of equal magnitude. As a result, their collective impact on the total eddy viscosity component is minimal or negative. Under homogeneous conditions, the tidal straining component dictates the structure of the eddy viscosity. Similarly, the cumulative effects of other components contribute negatively and minimally.*" "*The along-estuary non-dominant components exhibit consistent magnitudes and structures, irrespective of the presence or absence of wind forcing*,….."

Lines 717 – 763: The authors are encouraged to link the finding of the resent work to some other recent studies mentioned in the INTRODUCTION. Besides, the authors are encouraged to indicate how much the tidal straining component takes precedence over other factors in line 761 using numbers or percentages.

Response: The results of the current study have been contextualized with recent research highlighted in the introduction. (lines 788–791; lines 793–795; lines 798–800; lines 835–837). "*the primary mechanisms governing the LRV in the PRE under conditions of stratification and wind are elucidated, which has been not extensively explored in prior studies (Chu et al., 2022; Deng et al., 2022).*" "*Notably, the decomposition methodologies rooted in Lagrangian theory adopted in this work differ from earlier studies anchored in Eulerian theory (e.g., Burchard et al., 2011; Cheng et al., 2011; Wei et al., 2021).*" "*While many studies have focused on ERV in the PRE (e.g., Lai et al., 2018; Xu et al., 2021; Hong et al., 2022), research on LRV in the PRE remains limited, particularly regarding the dynamic mechanisms of LRV.*" "*Specifically, under stratified conditions, the turbulent mean component plays a dominant role in the total eddy viscosity component, which has not yet been studied in previous works (e.g., Burchard et al., 2023).*"

The magnitude of tidal straining has been quantitatively compared to other non-dominant components (lines 839–840). "*its magnitude is either several times or one order of magnitude bigger than the other components*."

Reference

Abbott, M. R.: Boundary layer effects in estuaries, J. Mar. Res., 18, 83–100, 1960.

Burchard, H., Bolding, K., Lange, X., Osadchiev, A.: Decomposition of Estuarine Circulation and Residual Stratification under Landfast Sea Ice, J. Phys. Oceanogr., 2023, 53(1), 57–80, 2023.

Burchard, H., Hetland, R. D., Schulz, E., Schuttelaars, H. M.: Drivers of residual estuarine circulation in tidally energetic estuaries: Straight and irrotational channels with parabolic cross section, J. Phys. Oceanogr., 41(3), 548–570, https://doi.org/10.1175/2010JPO4453.1, 2011.

Chen, S. M.: Water Exchange Due to Wind and Waves in a Monsoon Prevailing Tropical Atoll, J. Mar. Sci. Eng., 11(1), 109, 2023.

Cheng, P., Valle-Levinson, A., de Swart, H. E.: A numerical study of residual circulation induced by asymmetric tidal mixing in tidally dominated estuaries, J. Geophys. Res.: Oceans, 116(C1), https://doi.org/10.1029/2010JC006137, 2011.

Chu, N. Y., Liu, G. L., Xu, J., Yao, P., Du, Y., Liu, Z. Q., Cai, Z. Y.: Hydrodynamical transport structure and lagrangian connectivity of circulations in the Pearl River Estuary, Front. Mar. Sci., 9, 996551, https://doi.org/10.3389/fmars.2022.996551, 2022.

Deng, F. J., Jiang, W. S., Zong, X. L., Chen, Z. Y.: Quantifying the Contribution of Each Driving Force to the Lagrangian Residual Velocity in Xiangshan Bay, Front. Mar. Sci., 9, 901490, https://doi.org/10.3389/fmars.2022.901490, 2022.

Egbert, G. D., Erofeeva, S. Y.: Efficient inverse modeling of barotropic ocean tides, J. Atmos. Ocean. Technol., 19(2), 183–204, 2002.

Geyer, W. R., Ralston, D. K., Chen, J. L.: Mechanisms of exchange flow in an estuary with a narrow, deep channel and wide, shallow shoals, J. Geophys. Res.: Oceans, 125, e2020JC016092, https://doi.org/10.1029/2020-JC016092, 2020.

Hewageegana, V. H., Olabarrieta, M., Gonzalez-Ondina, J. M.: Main Physical Processes Affecting the Residence Times of a Micro-Tidal Estuary, J. Mar. Sci. Eng., 11(7): 1333, 2023.

Hong, B., Xue, H. L., Zhu, L. S., Xu, H. Z.: Climatic Change of Summer Wind Direction and Its Impact on Hydrodynamic Circulation in the Pearl River Estuary, J. Mar. Sci. Eng., 10, 10070842, https://doi.org/10.3390/jmse10070842, 2022.

Jiang, M. S.: Modeling Water Residence Time and Connectivity in the Northern Indian River Lagoon, Estuaries Coasts, 1-20, 2023.

Jiang, W. S., Feng, S. Z.: 3D analytical solution to the tidally induced Lagrangian residual current equations in a narrow bay, Ocean Dyn., 64, 1073–1091, https://doi.org/10.1007/s10236-014-0738-1, 2014.

Jongbloed, H., Schuttelaars, H. M., Dijkstra, Y. M., Donkers, P. B., Hoitink, A. J.: Influence of wind on subtidal salt intrusion and stratification in well-mixed and partially stratified estuaries, J. Phys. Oceanogr., 52(12), 3139–3158, https://doi.org/10.1175/JPO-D-21-0291.1, 2022.

Kukulka, T., Chant, R. J.: Surface convergence zones due to Lagrangian residual flow in tidally driven estuaries, J. Phys. Oceanogr., 53(2), 423-431, 2023.

Lai, W. F., Pan, J. Y., Devlin, A. T.: Impact of tides and winds on estuarine circulation in the Pearl River Estuary, Cont. Shelf Res., 168, 68–82, https://doi.org/10.1016/j.csr.2018.09.004, 2018.

Levitus, S., Antonov, J. I., Baranova, O. K., Boyer, T. P., Coleman, C. L., Garcia, H. E., Grodsky, A. I., Johnson, D. R., Locarnini, R. A., Mishonov, A. V., Reagan, J. R., Sazama, C. L., Seidov, D., Smolyar, I., Yarosh, E. S., Zweng, M. M.: The world ocean database. Data Science Journal, 12, WDS229-WDS234, 2013.

Li, S. Z., Zhang, Z. R., Zhou, M., Wang, C. N., Wu, H., Zhong, Y. S.: The role of fronts in horizontal transports of the Changjiang River plume in summer and the implications for phytoplankton blooms, J. Geophys. Res.: Oceans, 127(8), e2022JC018541 2022.

Lin, L., Liu, D. Y., Fu, Q. J., Guo, X. Y., Liu, G. L., Liu, H., Wang, S. L.: Seasonal variability of water residence time in the Subei Coastal Water, Yellow Sea: The joint role of tide and wind, Ocean Model., 180, 102137, https://doi.org/10.1016/j.ocemod.2022.102137, 2022.

Mears, C., Lee, T., Ricciardulli, L., Wang, X. C., Wentz, F.: Rss cross-calibrated multi-platform (Ccmp) 6-hourly ocean vector wind analysis on 0.25 deg grid, version 3.0, Remote Sens., Syst, 2022.

NOAA National Geophysical Data Center.: 2-minute Gridded Global Relief Data (ETOPO2) v2. NOAA National Centers for Environmental Information, https://doi.org/10.7289/V5J1012Q, 2006.

Pan, J. Y., Gu, Y. Z.: Cruise observation and numerical modeling of turbulent mixing in the Pearl River estuary in summer, Cont. Shelf Res., 120, 122-138, 2016.

Pan, J. Y., Gu, Y. Z., Wang, D. X.: Observations and numerical modeling of the Pearl River plume in summer season, J. Geophys. Res.: Oceans, 119, 2480–2500, https://doi.org/10.1002/2013JC009042, 2014.

Ren, L., Yang, L. N., Pan, G. W., Zheng, G., Zhu, Q., Wang, Y. Q., Zhu, Z. C., Hartnett, M.: Characterizing Residual Current Circulation and Its Response Mechanism to Wind at a Seasonal Scale Based on High-Frequency Radar Data, Remote Sens., 14, 14184510, https://doi.org/10.3390/rs14184510, 2022.

Soto-Riquelme, C., Pinilla, E., Ross, L.: Wind influence on residual circulation in Patagonian channels and fjords, Cont. Shelf Res., 254, 104905, 2023.

Verspecht, F., Rippeth, T. P., Howarth, M. J., Souza, A. J., Simpson, J. H., Burchard, H.: Processes impacting on stratification in a region of freshwater influence: Application to Liverpool Bay, J. Geophys. Res.: Oceans, 114(C11), https://doi.org/10.1029/2009JC005475, 2009.

Wei, X. Y., Schuttelaars, H. M., Williams, M. E., Brown, J. M., Thorne, P. D., Amoudry, L. O.: Unraveling interactions between asymmetric tidal turbulence, residual circulation, and salinity dynamics in short, periodically weakly stratified estuaries, J. Phys. Oceanogr., 51(5), 1395–1416, https://doi.org/10.1175/JPO-D-20-0146.1, 2021.

Xu, H. Z., Shen, J., Wang, D. X., Luo, L., Hong, B.: Nonlinearity of subtidal estuarine circulation in the Pearl River Estuary, China, Front. Mar. Sci., 8, 629403, https://doi.org/10.3389/fmars.2021.629403, 2021.

Young, J. S., Hoon, Y. K., Jongseong, R., Kyung, H. H.: Wind-induced switch of estuarine residual circulations and sediment transport in microtidal bay, Estuar. Coast. Shelf Sci., 288, 2023.

Yu, J. Z., Zhang, X. Q., Sheng, X. X., Jiang, W. S.: Mass transport pattern and mechanism in the tide-dominant Bohai Sea, Ocean Model., 182, 2023.

Zhang, D. Q., Pang, C. G., Liu, Z. L., Jiang, J. B.: Winter and summer sedimentary dynamic process observations in the sea area off Qinhuangdao in the Bohai Sea, China, Front. Earth Sci., 11, 1097033, https://doi.org/10.3389/feart.2023.1097033, 2023.

Zimmerman, J. T. F.: On the Euler-Lagrange transformation and the Stokes' drift in the presence of oscillatory and residual currents, Deep-Sea Res., 26A, 505–520, 1979.

Figures

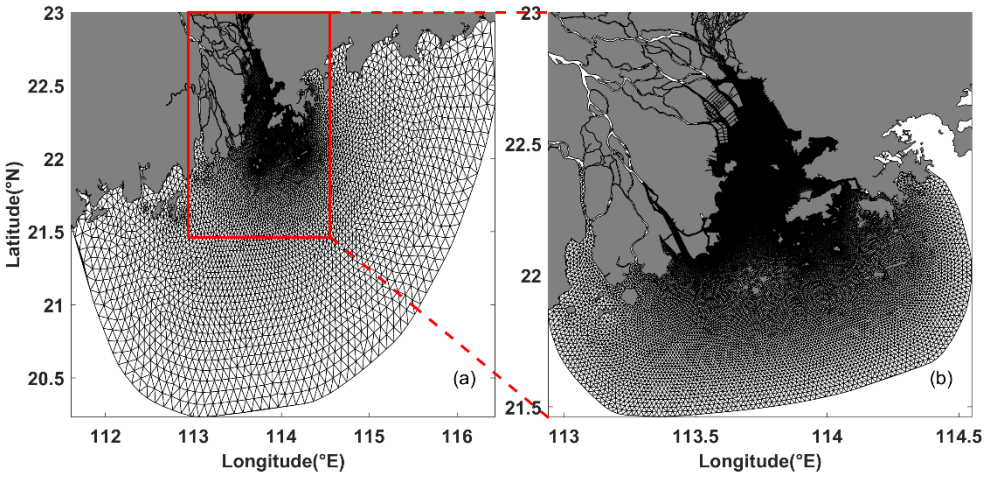

Figure 1 (a) Coarse mesh model, **(b)** fine mesh model.

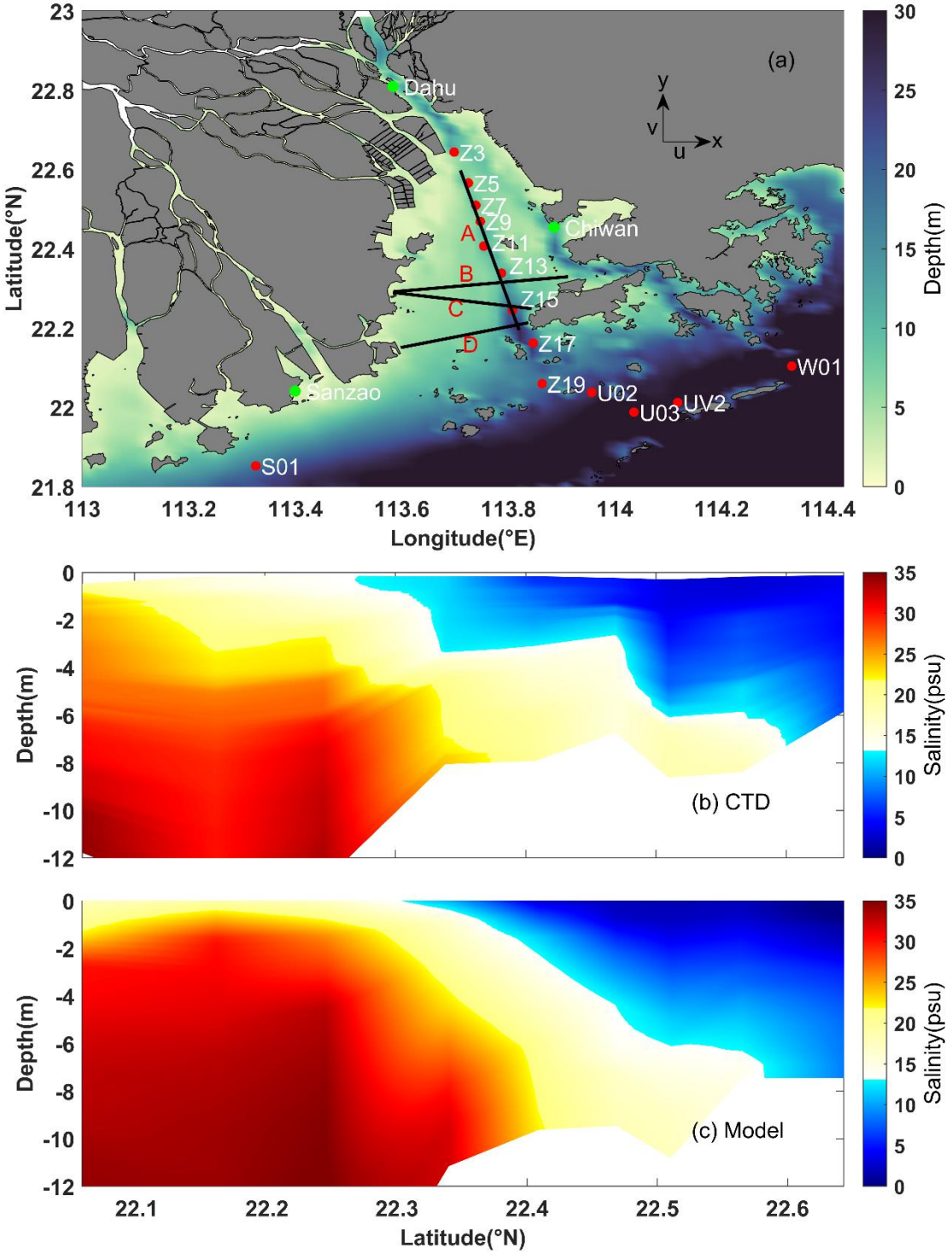

Figure 2 (a) Bathymetry of the model domain. Black lines mark sections for result analysis. Green dots indicate tide gauge stations for elevation validation, and red dots indicate CTD positions for salinity verification. **(b)** Along-estuary salinity profiles based on CTD depth-profiled data, closely aligned with Section A; **(c)** salinity outputs from the numerical model.

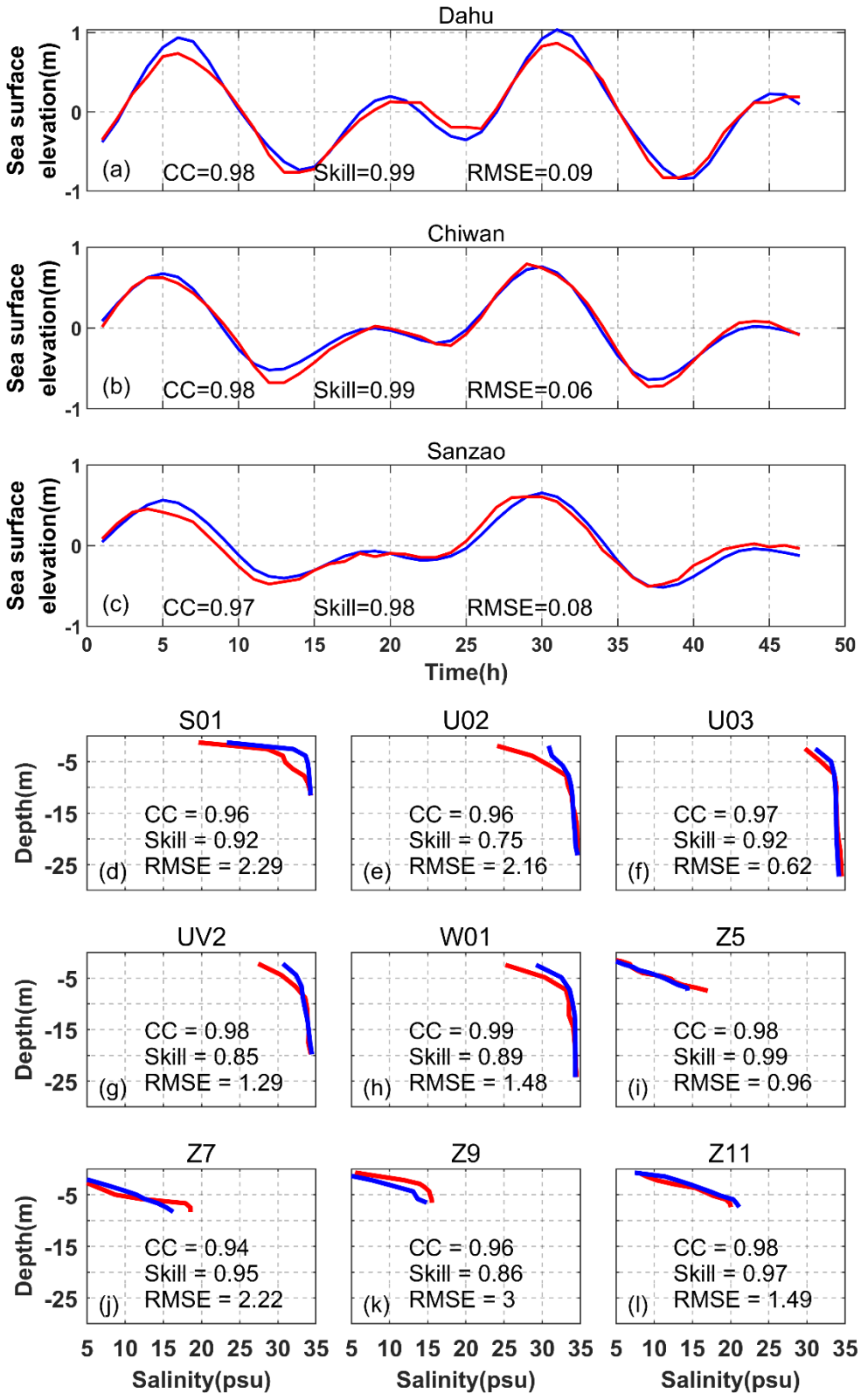

Figure 3 Comparisons between the observed (red line) and modeled (blue line) elevation and salinity. The three parameters including CC, Skill, and RMSE are calculated at each station.

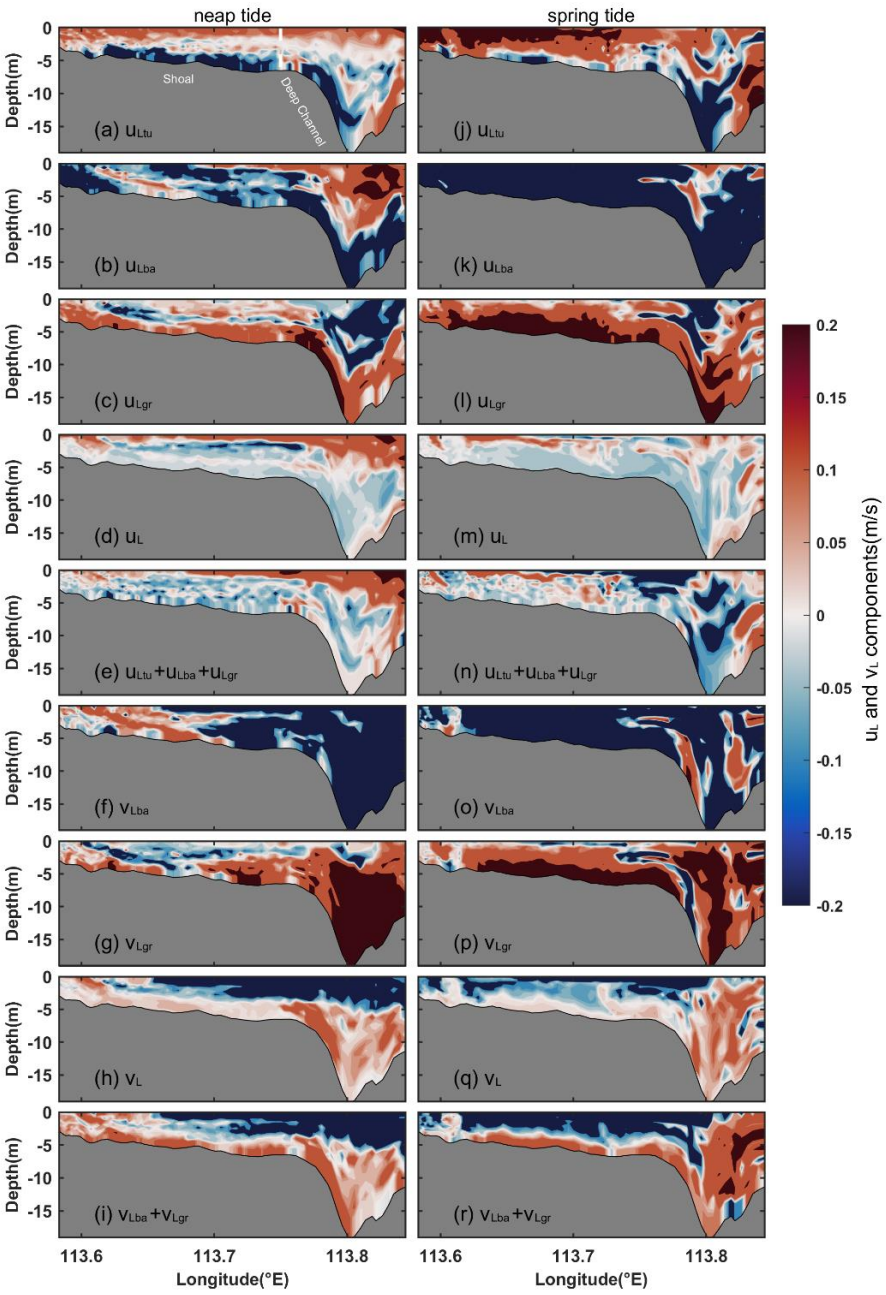

Figure 4 Dominant components of u_L and v_L in Section C for Case 1. For cross-estuary components: **(a, j)** eddy viscosity component (u_{Ltu}), **(b, k)** barotropic component (u_{Lba}), **(c, l)** baroclinic component (u_{Lgr}), **(d, m)** total LRV (u_L) directly obtained by the model, and **(e, n)** cumulative sum of u_{Ltu}, u_{Lba}, and u_{Lgr}. For along-estuary components: **(f, o)** barotropic pressure gradient component (v_{Lba}), **(g, p)** baroclinic pressure gradient component (v_{Lgr}), **(h, q)** total LRV (v_L) obtained directly by the model, and **(i, r)** cumulative sum of v_{Lba} and v_{Lgr}. The components during **(a–i)** represent neap tides, while those during **(j–r)** represent spring tides. For cross-estuary components, red shading indicates eastward flow, and blue shading indicates westward flow. For along-estuary components, red shading signifies inflow, while blue shading denotes outflow.

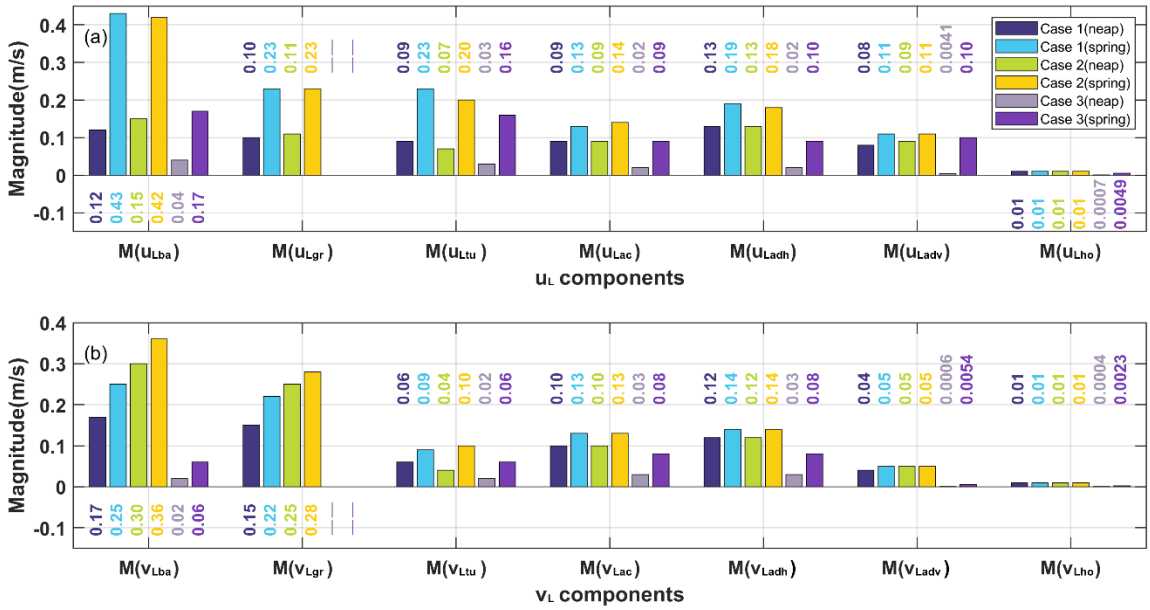

Figure 5 Bar charts for the magnitude of each component of u_L and v_L.

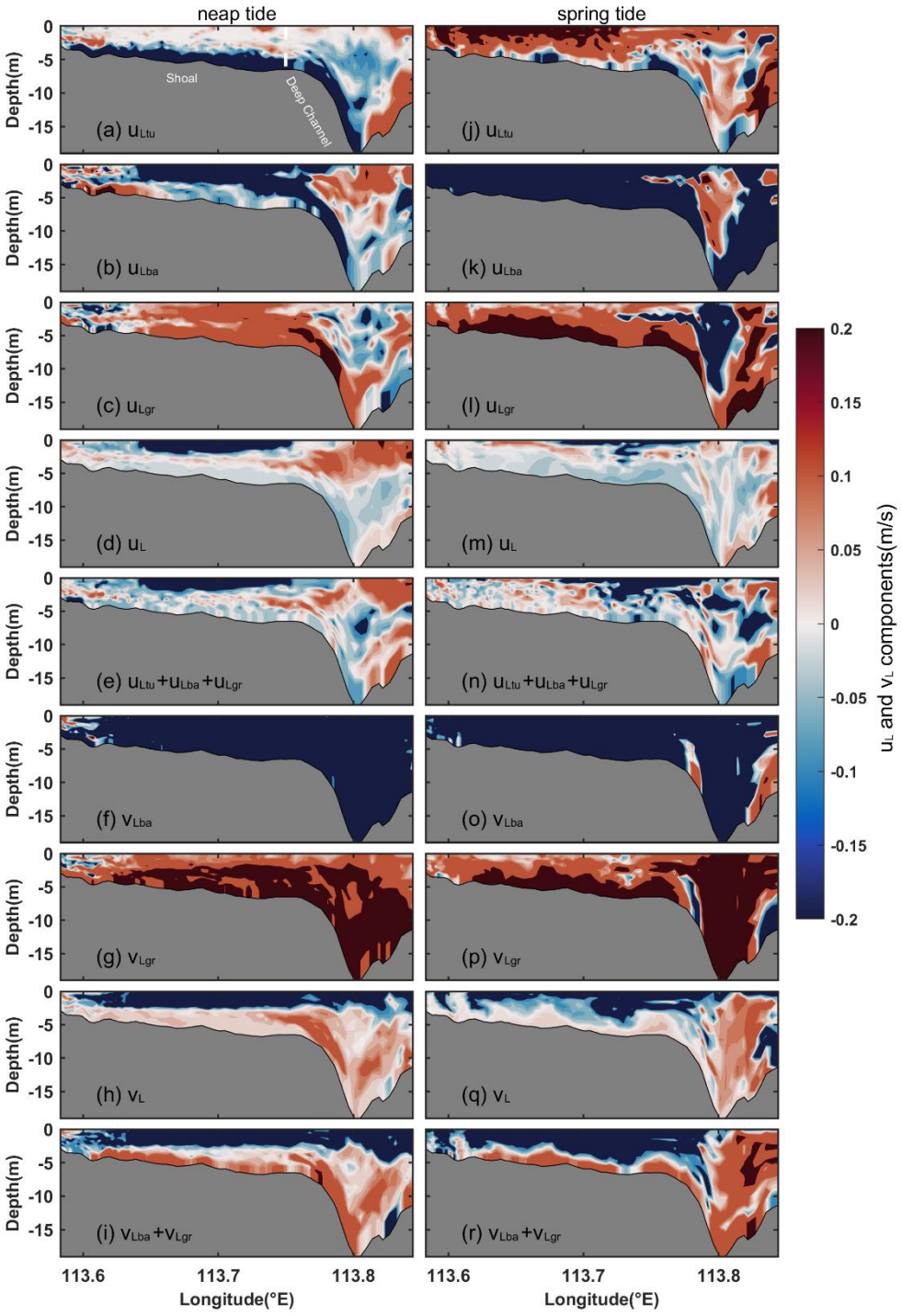

Figure 6 Same as Fig. 4, but for Case 2 without wind forcing.

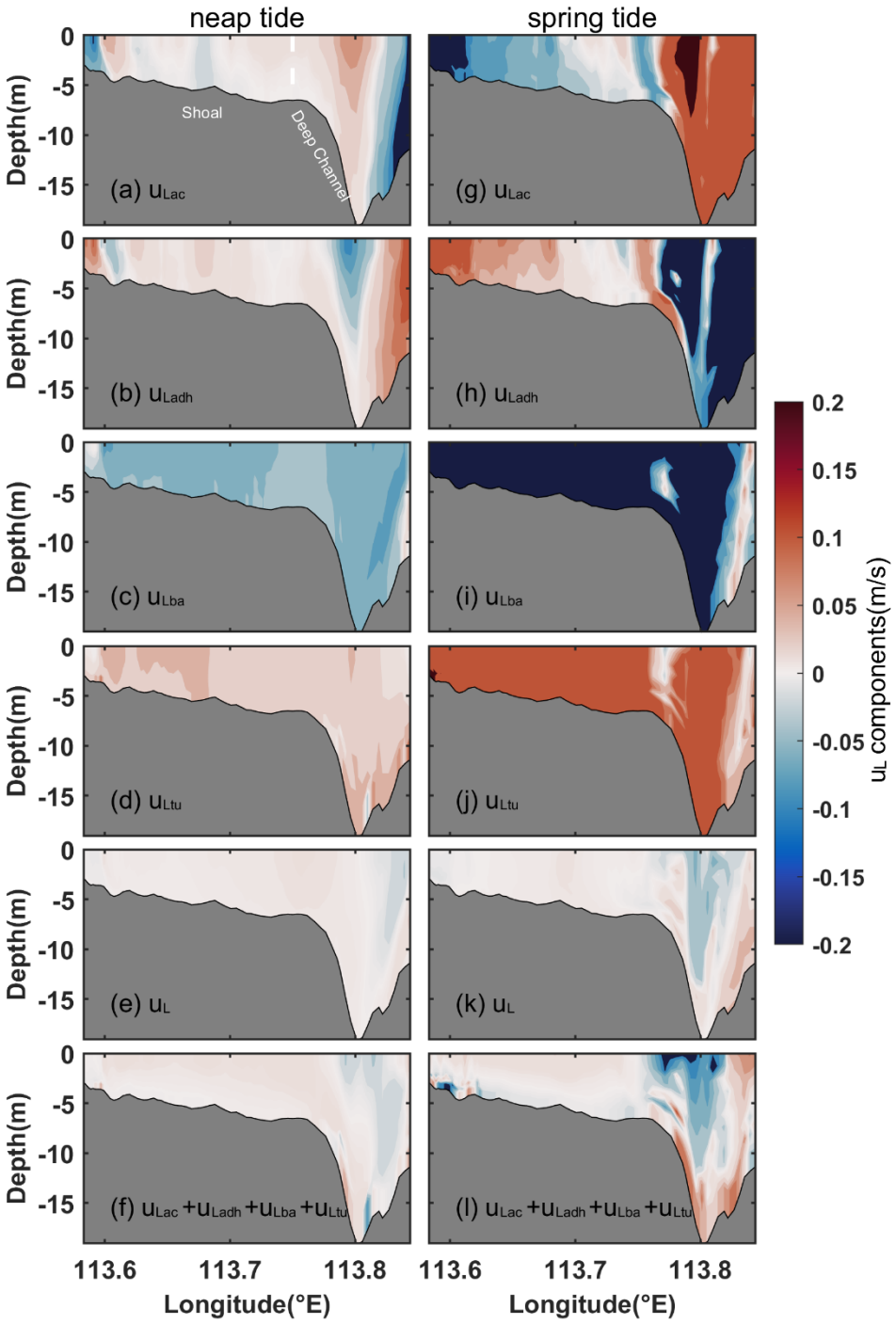

Figure 7 Dominant components of u_L in Section C for Case 3. **(a, g)** Local acceleration component (u_{Lac}), **(b, h)** horizontal nonlinear advection component (u_{Ladh}), **(c, i)** barotropic pressure gradient component (u_{Lba}), **(d, j)** eddy viscosity component (u_{Ltu}), **(e, k)** the total LRV (u_L) obtained directly by the model, and **(f, l)** the sum of u_{Lac}, u_{Ladh}, u_{Lba}, and u_{Ltu} during **(a–f)** neap and **(g–l)** spring tides, respectively. Red shading represents eastward flow and blue shading represents westward flow.

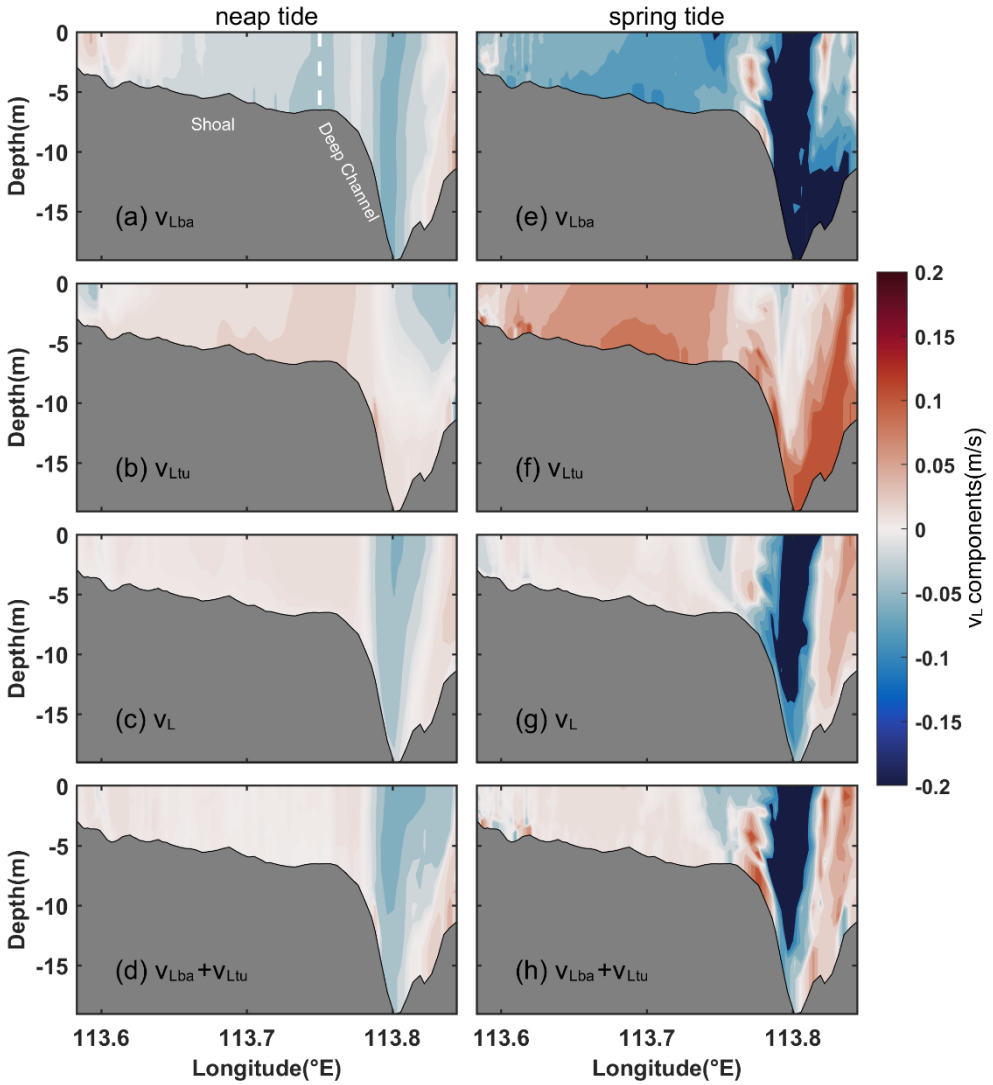

Figure 8 Dominant components of v_L in Section C for Case 3. **(a, e)** Barotropic pressure gradient component (v_{Lba}), **(b, f)** eddy viscosity component (v_{Ltu}), **(c, g)** total LRV obtained directly by the model, and **(d, h)** the sum of v_{Lba} and v_{Ltu} during **(a–d)** neap and **(e–h)** spring tides, respectively. Red shading represents inflow, and blue shading represents outflow.

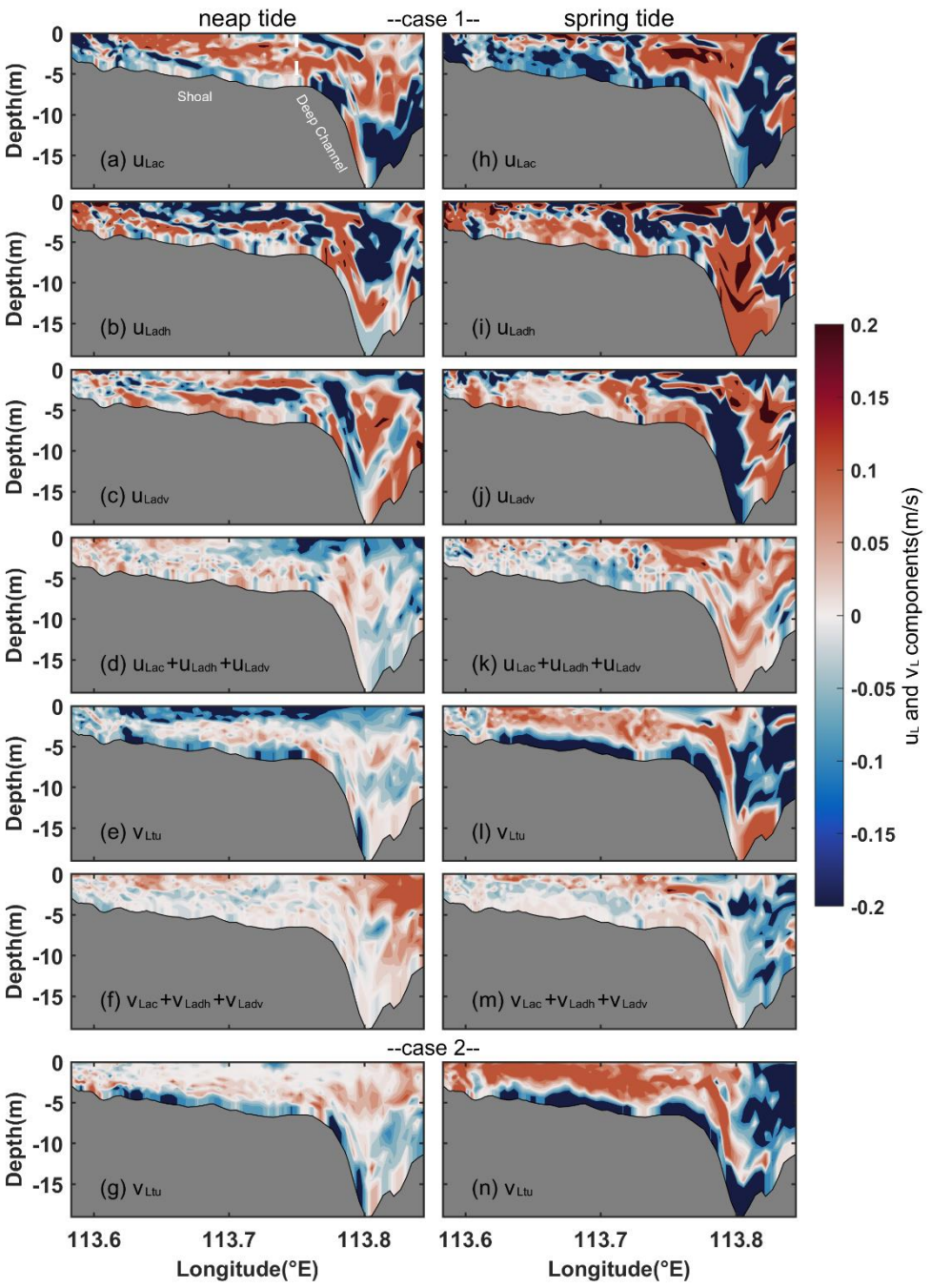

Figure 9 Non-dominant components of u_L and v_L in Section C for Cases 1 and 2. For cross-estuary components in Case 1: **(a, h)** local acceleration component (u_{Lac}), **(b, i)** horizontal nonlinear advection component (u_{Ladh}), **(c, j)** vertical nonlinear advection component (u_{Ladv}), and **(d, k)** the sum of u_{Lac}, u_{Ladh}, and u_{Ladv} during **(a–d)** neap and **(h–k)** spring tides, respectively; for along-estuary components in Case 1: **(e, l)** eddy viscosity component (v_{Ltu}), **(f, m)** the sum of v_{Lac}, v_{Ladh}, and v_{Ladv} during **(e, f)** neap and **(l, m)** spring tides, respectively. Along-estuary **(g, n)** eddy viscosity component (v_{Ltu}) in Case 2 during **(g)** neap and **(n)** spring tides, respectively. The shading follows the same indications as presented in Fig. 1.

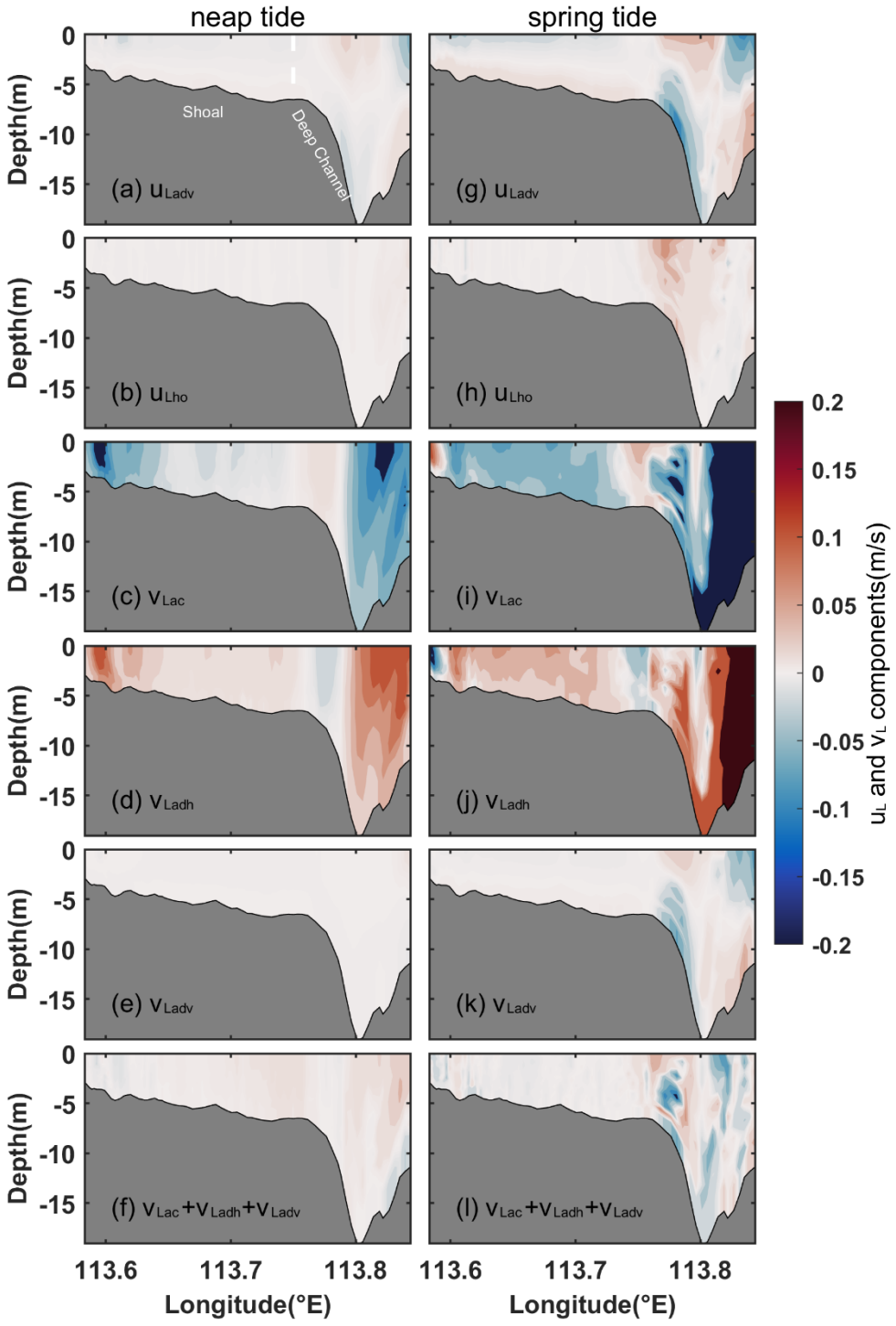

Figure 10 Non-dominant components of u_L and v_L in Section C for Case 3. For cross-estuary components: **(a, g)** vertical nonlinear advection component (u_{Ladv}), **(b, h)** horizontal diffusion component (u_{Lho}); for along-estuary components: **(c, i)** local acceleration component (v_{Lac}), **(d, j)** horizontal advection component (v_{Ladh}), **(e, k)** vertical advection component (v_{Ladv}), and **(f, l)** the sum of v_{Ladc}, v_{Ladh} and v_{Ladv}, during **(a–f)** neap and **(g–l)** spring tides, respectively. The shading follows the same indications as presented in Fig. 1.

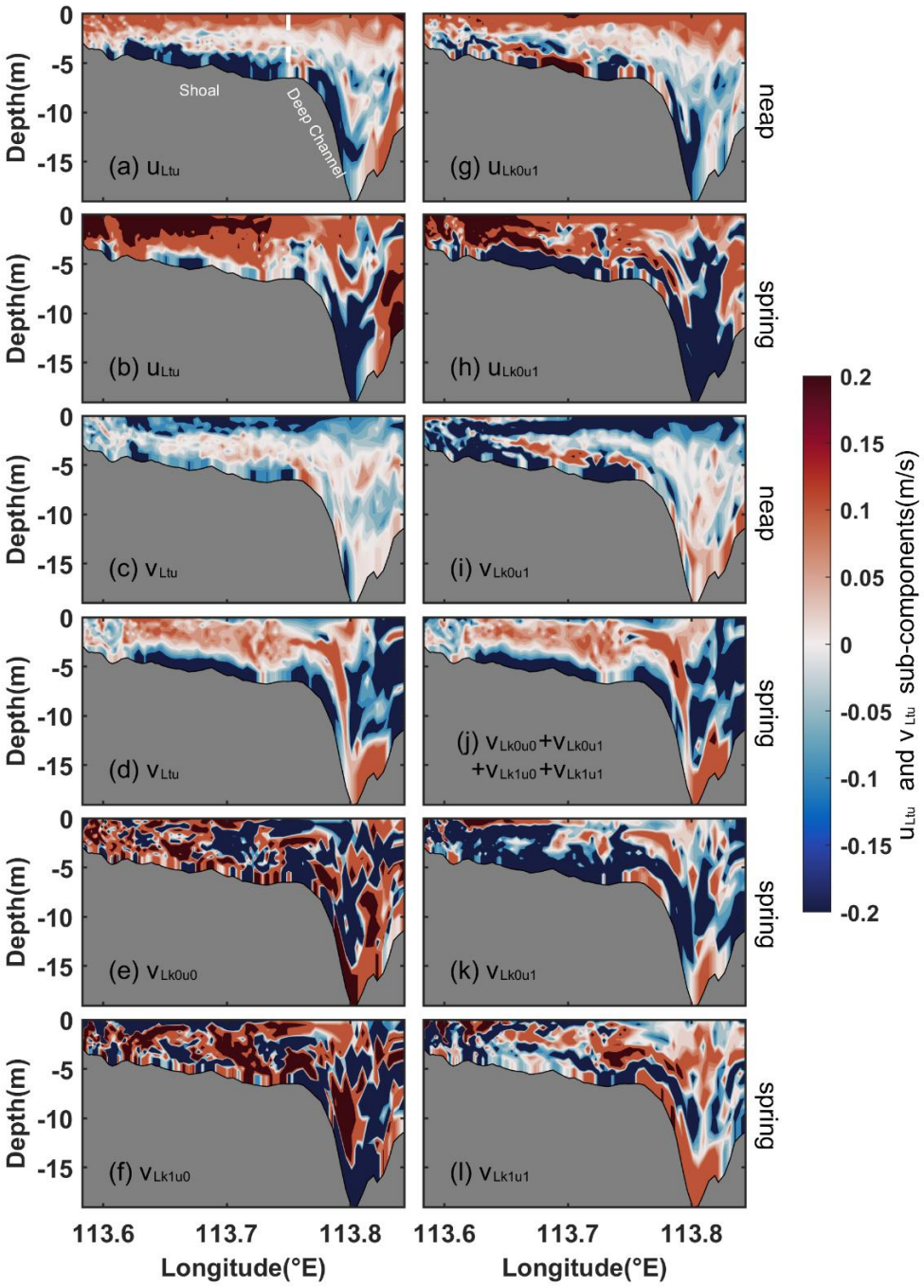

Figure 11 Vertical section of cross-estuary (u_{Ltu}) and along-estuary (v_{Ltu}) eddy viscosity components along with their corresponding dominant subcomponents in Section C for Case 1. The u_{Ltu} during **(a)** neap and **(b)** spring tides, and **(g, h)** the corresponding turbulent mean component (u_{Lk0u1}). **(c)** v_{Ltu} and **(i)** the corresponding turbulent mean component (v_{Lk0u1}) during neap tides, and **(d)** v_{Ltu} and **(j)** the sum of four dominant subcomponents **(e, f, k, and l)** during spring tides. The shading follows the same indications as presented in Fig. 1.

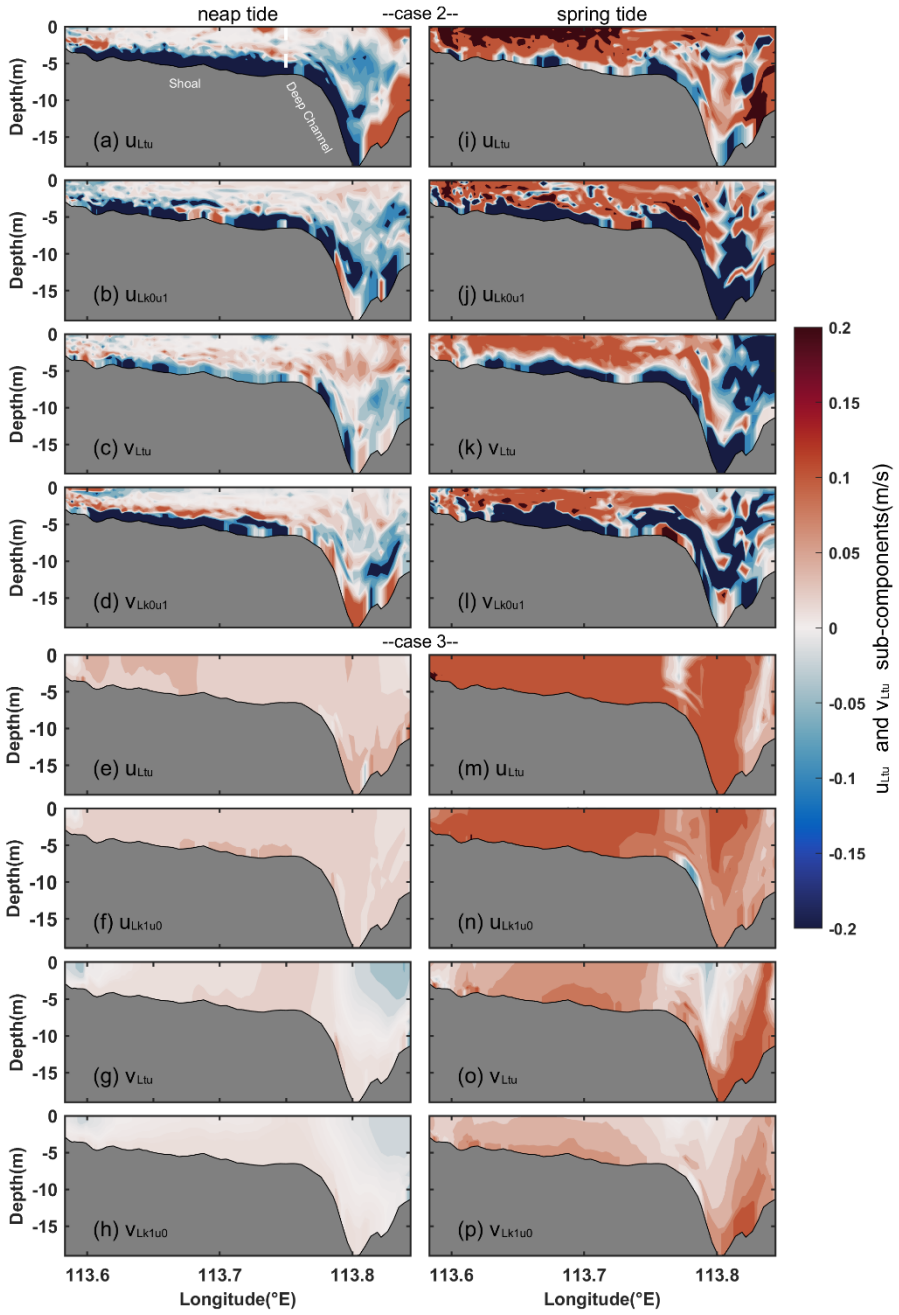

Figure 12 The structure of cross-estuary (u_{Ltu}) and along-estuary (v_{Ltu}) eddy viscosity components and the corresponding dominant components in Section C for Cases 2 **(a–d and i–l)** and 3 **(e–h, and m–p)**. For Case 2: the u_{Ltu} during **(a)** neap and **(i)** spring tides, and **(b, j)** the corresponding turbulent mean component (u_{Lk0u1}); the v_{Ltu} during **(c)** neap and **(k)** spring tides, and **(d, l)** the corresponding turbulent mean component (v_{Lk0u1}). For Case 3: the u_{Ltu} during **(e)** neap and **(m)** spring tides, and **(f, n)** the corresponding tidal straining component (u_{Lk1u0}); the v_{Ltu} during **(g)** neap and **(o)** spring tides, and **(h, p)** the corresponding tidal straining component (v_{Lk1u0}). The shading follows the same indications as presented in Fig. 1.

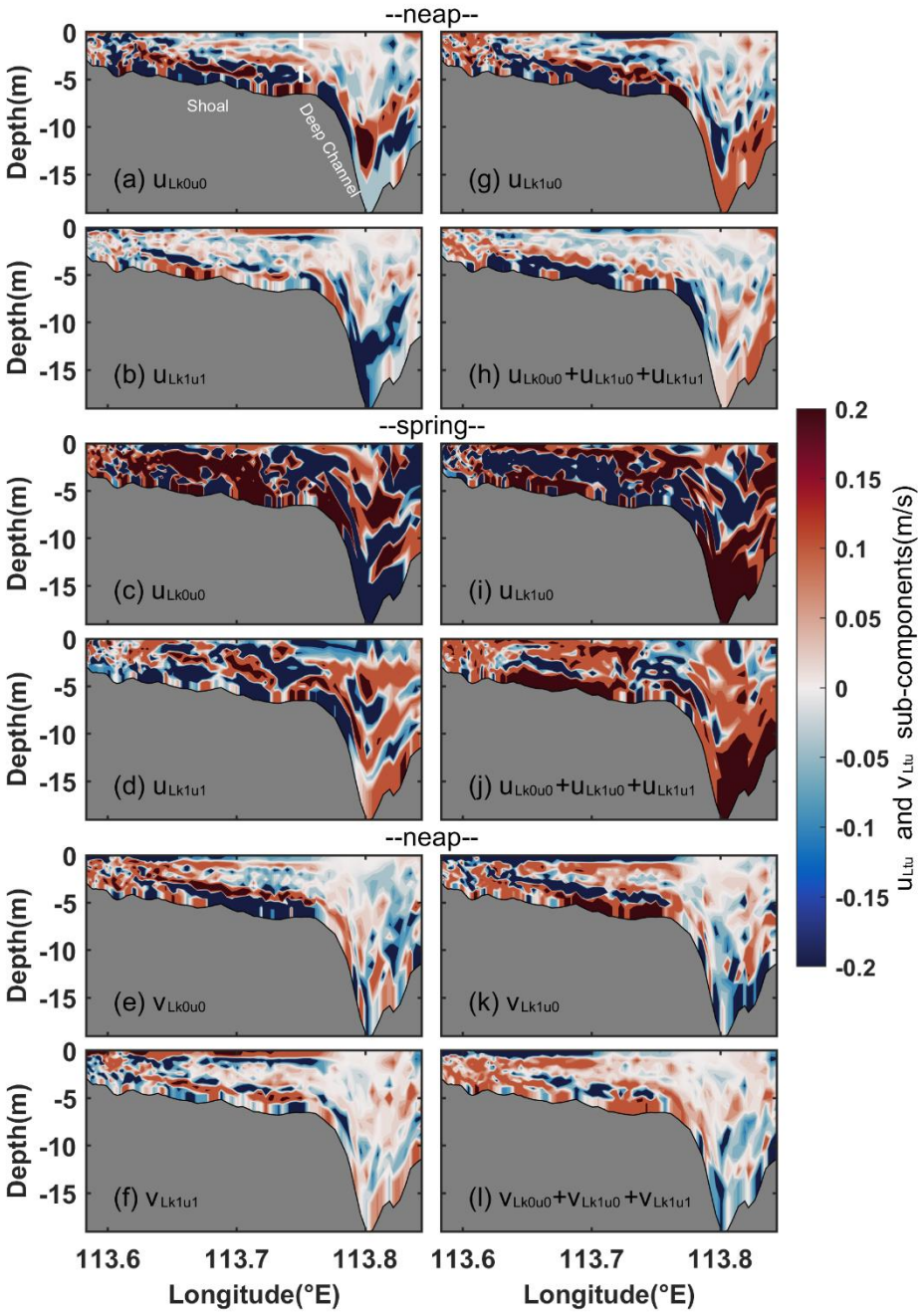

Figure 13 Vertical profiles of non-dominant subcomponents of cross-estuary (u_{Ltu}) and along-estuary (v_{Ltu}) eddy viscosity components for Case 1. For cross-estuary subcomponents: **(a, c)** coupled component of the tidal-average eddy viscosity and velocity gradient oscillation (u_{Lk0u0}), **(g, i)** tidal straining component (u_{Lk1u0}), **(b, d)** coupled component of eddy viscosity oscillation and the tidal-average velocity gradient (u_{Lk1u1}), **(h, j)** the sum of the three subcomponents during neap **(a, b, g, h)** and spring **(c, d, i, j)** tides, respectively. **(e, k, f, l)** Corresponding along-estuary eddy viscosity subcomponents during neap tides.

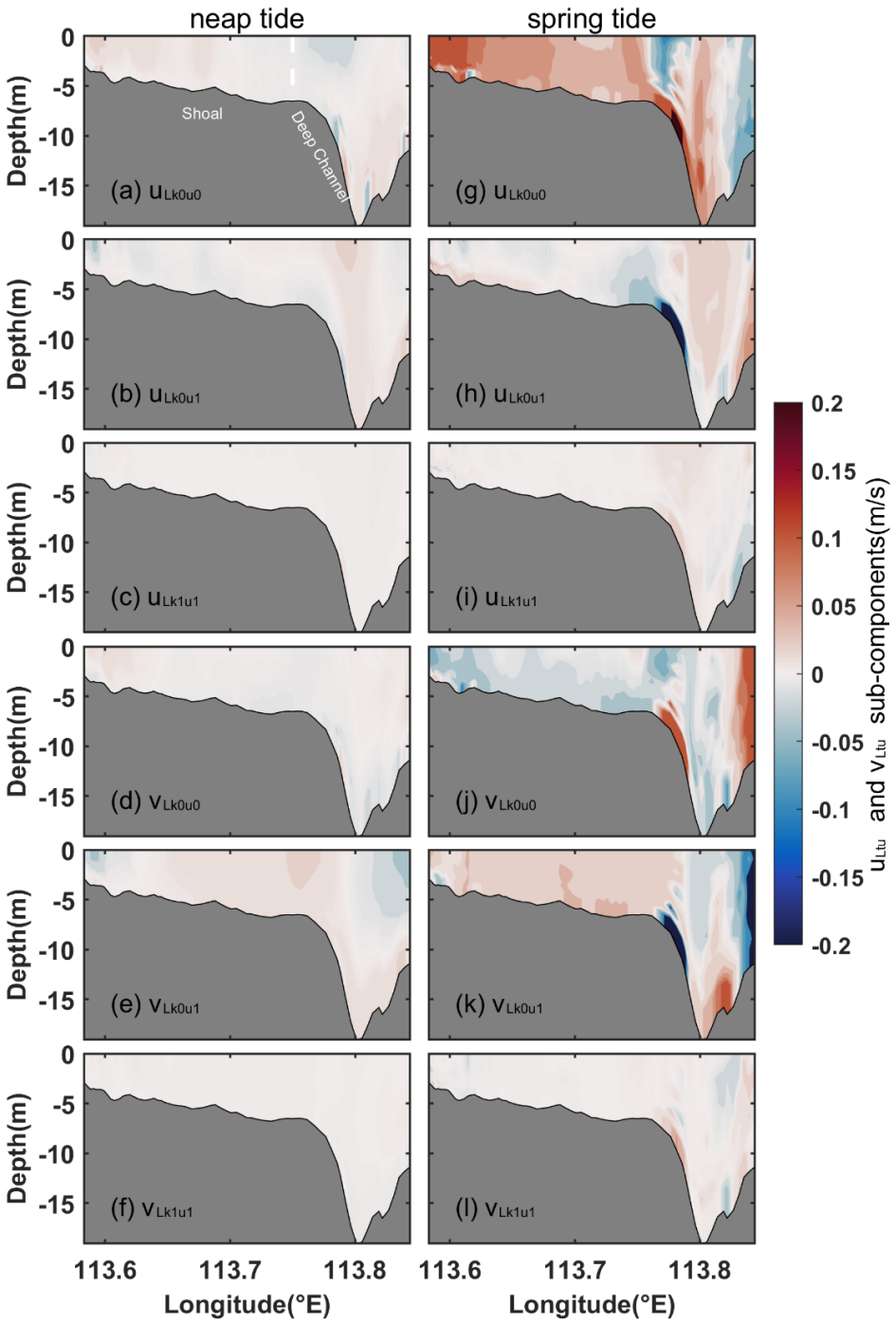

Figure 14 Vertical profiles of non-dominant subcomponents of cross-estuary (u_{Ltu}) and along-estuary (v_{Ltu}) eddy viscosity components for Case 3. For cross-estuary subcomponents: **(a, g)** coupled component of the tidal-average eddy viscosity and velocity gradient oscillation (u_{Lk0u0}), **(b, h)** turbulent mean component (u_{Lk0u1}), **(c, i)** coupled component of eddy viscosity oscillation and the tidal-average velocity gradient (u_{Lk1u1}) during neap **(a–c)** and spring **(g–i)** tides, respectively. **(d, j, e, k, f, l)** Corresponding along-estuary eddy viscosity subcomponents.

Review 2

This study investigates residual circulation in the Peral River estuary using the Lagrangian residual velocity. It evaluated the contribution of each component of the Lagranigian residual velocity and in particular analyzed the four components of turbulent mean component. The results are interesting. I have few concerns and hope they can be clarified before publication of this manuscript in OS.

Response: We extend our sincere appreciation for your dedicated and insightful review of our manuscript. Your meticulous examination and thoughtful comments have been invaluable in refining and strengthening our work.

1. The decomposition of Lagrangian residual velocity

The decomposition method basically is to use the Coriolis term in momentum balance in which each term is divided by the Coriolis parameter. Because the velocity in the Coriolis term is cross correspondence, i.e. u is in the momentum balance of v, and v is in the momentum balance of u. Thus, the physical meaning of each velocity component is hard to explain. For example, the baroclinic pressure gradient component of u is related to density gradient in y direction. That doesn't make sense. Furthermore, if there is no Coriolis force, how do you decompose the velocity?

Response: Thank you for your professional comments on this research and also thanks for providing this opportunity to explain our work.

The decomposition method has physical meaning when the Coriolis force is important. The Pearl River Estuary (PRE) features a relatively wide expanse, measuring 20–60 km in width in the middle and lower regions, away from the river discharge input nodes, and extending over a length of 70 km. The Rossby number is approximately 0.2 in the Pearl River Estuary (PRE), similar to that calculated by Li et al. (2023), signifying the prominence of the Coriolis force in the region's dynamics. The baroclinic Rossby deformation radius is estimated to be approximately 12–16 km, a range similar to the findings of Pan et al. (2014), suggesting the necessity to account for the rotational effect of the Earth. Lai et al. (2018) highlighted that the influence of the Coriolis force in the PRE is substantial with its effect extending to the bottom layer when compared to vertical mixing, and baroclinic and barotropic momentum when analyzing the Eulerian average momentum equation. Chen et al. (2019) indicated that in the depth-integrated momentum balance prior to a storm in the PRE, local momentum balance primarily involves the pressure gradient force, the Coriolis force, and bottom stress. Synthesizing current and prior research, it becomes apparent that the Coriolis force is a predominant factor influencing the dynamics of the PRE. The aforementioned discussion accentuates the criticality and practicality of employing decomposition methods in such analytical contexts.

The physical dynamics within the Pearl River Estuary (PRE) can be elucidated as follows: the cross-estuary Lagrangian mean momentum equation is characterized by quasi-geostrophic balance, whereas the along-estuary Lagrangian mean momentum equation conforms to a blend of quasi-geostrophic and Ekman balances. That is because the cross-estuary Lagrangian Residual Velocity (LRV) is predominantly influenced by the interplay of barotropic and baroclinic pressure gradient components, alongside eddy viscosity components. Conversely, the along-estuary LRV is chiefly propelled by barotropic and baroclinic pressure gradient components. The aggregate of local acceleration, horizontal nonlinear advection, and vertical nonlinear advection terms make a lesser and inverse contribution to the overall LRV. The input from the horizontal diffusion component is minimal, verging on negligible, as demonstrated in Fig. A1. Consequently, the Lagrangian mean momentum equations can be approximately simplified as follows:

$$-fv_L \approx -\underbrace{\langle g\frac{\partial \zeta}{\partial x}\rangle}_{1} - \underbrace{\langle \frac{g}{\rho_0}\left(D\int_\sigma^0 \frac{\partial \rho}{\partial x}d\sigma_1 + \frac{\partial D}{\partial x}\int_\sigma^0 \sigma_1 \frac{\partial \rho}{\partial \sigma_1}d\sigma_1\right)\rangle}_{2}, \tag{A1}$$

$$fu_L \approx \underbrace{-\langle g\frac{\partial \zeta}{\partial y}\rangle}_{1}\underbrace{-\langle \frac{g}{\rho_0}\left(D\int_\sigma^0 \frac{\partial \rho}{\partial y}d\sigma_1 + \frac{\partial D}{\partial y}\int_\sigma^0 \sigma_1 \frac{\partial \rho}{\partial \sigma_1}d\sigma_1\right)\rangle}_{2} + \underbrace{\langle \frac{1}{D^2}\frac{\partial}{\partial \sigma}\left(v_h\frac{\partial v}{\partial \sigma}\right)\rangle}_{3}, \tag{A2}$$

where The symbol <> represents the Lagrangian mean, the terms on the left-hand side of Eqs. (A1) and (A2) denote the Lagrangian mean Coriolis force. Conversely, the first and second terms on the right-hand side of these equations correspond to the Lagrangian mean barotropic and baroclinic pressure gradient forces, respectively. Furthermore, the third term on the right-hand side of Eq. (A2) represents the Lagrangian mean eddy viscosity term.

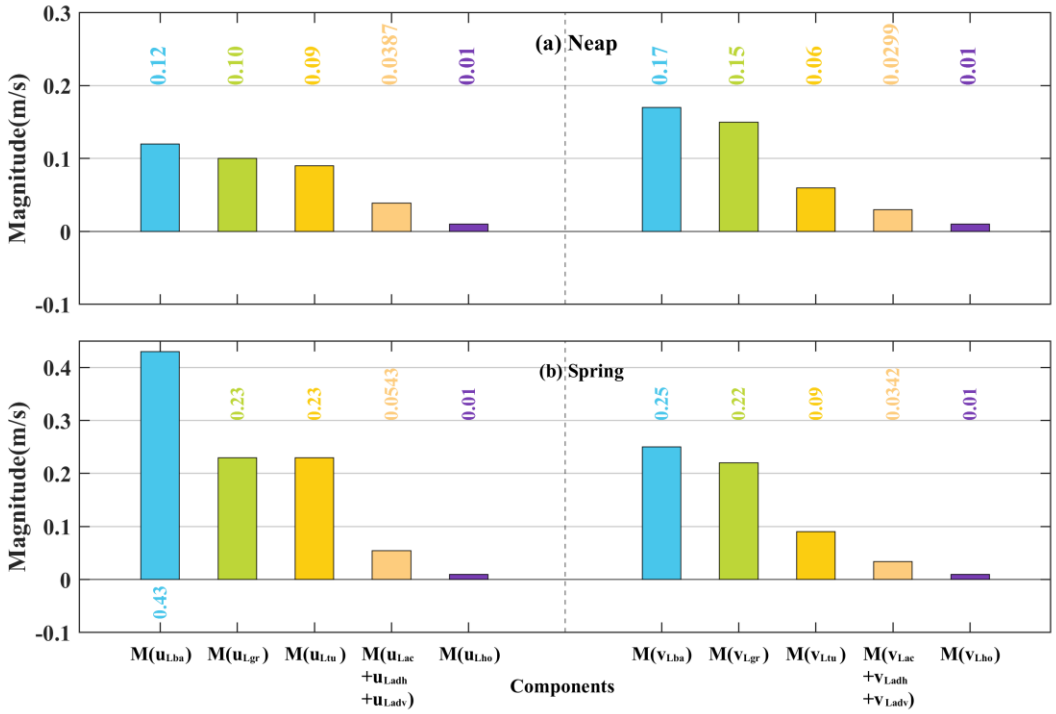

Figure A1 Bar charts for the magnitudes of individual components of u_L and v_L. The notation M(·) corresponds to the mean of absolute values for the components discussed in Section C. Specifically, M(u_{Lba}) quantifies the mean of the absolute values for the barotropic component, M(u_{Lgr}) for the baroclinic component, and M(u_{Ltu}) for the eddy viscosity component. Additionally, M(u_{Lac}+u_{Ladh}+u_{Ladv}) aggregates the mean of absolute values for the combined local acceleration, horizontal advection, and vertical advection components. M(u_{Lho}) calculates the mean of the absolute values for the horizontal diffusion component. Corresponding measurements for along-estuary components, namely M(v_{Lba}), M(v_{Lgr}), M(v_{Ltu}), M(v_{Lac}+v_{Ladh}+v_{Ladv}), and M(v_{Lho}), are analogously defined and follow a similar interpretative framework.

Analogous decomposition methodologies have been implemented in prior studies, notably in the research conducted by Wu et al. (2018). Their investigation delineated that a pivotal premise of Eq. (6) hinges on the assumption of a minimal Rossby number, thereby emphasizing the paramount importance of Coriolis forces within the framework of Eulerian residual transport dynamics analysis. The equation for V_R (Wu et al., 2018) is as follows:

$$V_R = -\frac{1}{fH}\left\langle u_s \frac{\partial \eta}{\partial t}\right\rangle + \frac{\langle ADV\rangle}{fH} + \frac{g}{2fH}\frac{\partial\langle\eta^2\rangle}{\partial x} + \frac{g}{f}\frac{\partial\langle\eta\rangle}{\partial x} - \frac{\langle\tau_x^s\rangle}{\rho fH} + \frac{\langle\tau_x^b\rangle}{\rho fH} + \mathrm{Re}\ si, \qquad (6)$$

where V_R represents the north-south component of Eulerian residual transport, and the angle brackets denote the Eulerian mean. The first two terms on the right side of equation (6) represent local acceleration and the nonlinear advection components, respectively; the third and fourth terms correspond to the pressure gradient forcing; the fifth and sixth terms represent surface wind stress and bottom friction forcing, respectively; the seventh term encompasses other components.

The decomposition methodologies present distinct advantages for elucidating the dynamics of Lagrangian Residual Velocity (LRV) within generally or weakly nonlinear systems. This significance stems from the absence of comprehensive analytical solutions and definitive governing equations for LRV in generally nonlinear contexts, coupled with the constraints of analytical solutions in weakly nonlinear frameworks (Jiang and Feng, 2014; Cui et al., 2019; Chen et al., 2020).

In scenarios where the Coriolis force is negligible, the Lagrangian mean momentum equations remain applicable for primary momentum balance analysis. However, these equations are inadequate for the detailed dissection of each LRV component. Notably, in circumstances where the Coriolis effect is minimally impactful, the methodologies employed for LRV decomposition may demonstrate variability, contingent upon the dominant momentum balances. This underscores the necessity for expanded investigation in future scholarly endeavors.

The relative contents have been added to the revised manuscript (lines 697–715; lines 765–776): "*The Pearl River Estuary (PRE) features a relatively wide expanse, measuring 20–60 km in width in the middle and lower regions, away from the river discharge input nodes, and extending over a length of 70 km. The Rossby number is approximately 0.2 in the Pearl River Estuary (PRE), similar to that calculated by Li et al. (2023), signifying the prominence of the Coriolis force in the region's dynamics. The baroclinic Rossby deformation radius is estimated to be approximately 12–16 km, a range similar to the findings of Pan et al. (2014), suggesting the necessity to account for the rotational effect of the Earth. Lai et al. (2018) highlighted that the influence of the Coriolis force in the PRE is substantial with its effect extending to the bottom layer when compared to vertical mixing, and baroclinic and barotropic momentum when analyzing the Eulerian average momentum equation. Chen et al. (2019) indicated that in the depth-integrated momentum balance prior to a storm in the PRE, local momentum balance primarily involves the pressure gradient force, the Coriolis force, and bottom stress. Synthesizing current and prior research, it becomes apparent that the Coriolis force is a predominant factor influencing the dynamics of the PRE. This assertion is corroborated by Wu et al. (2018), who contend that the decomposition approach to Eulerian residual transport assumes particular significance in scenarios marked by a notable presence of Coriolis forces, as evidenced by a small Rossby number. The aforementioned discussion accentuates the criticality and practicality of employing decomposition methods in such analytical contexts.*" "*The decomposition methodologies present distinct advantages for elucidating the dynamics of Lagrangian Residual Velocity (LRV) within generally or weakly nonlinear systems. This significance stems from the absence of comprehensive analytical solutions and definitive governing equations for LRV in generally nonlinear contexts, coupled with the constraints of analytical solutions in weakly nonlinear frameworks (Jiang and Feng,*

2014; Cui et al., 2019; Chen et al., 2020). In scenarios where the Coriolis force is negligible, the Lagrangian mean momentum equations remain applicable for primary momentum balance analysis. However, these equations are inadequate for the detailed dissection of each LRV component. Notably, in circumstances where the Coriolis effect is minimally impactful, the methodologies employed for LRV decomposition may demonstrate variability, contingent upon the dominant momentum balances. This underscores the necessity for expanded investigation in future scholarly endeavors."

2. The decomposition of eddy viscosity component (i.e. section 2.1)

How do you decompose the velocity and eddy viscosity into tidal average and tidal oscillation parts? Is the tidal average Eulerian or Lagrangian average? If it is Eulerian average, what is the physical meaning of the decomposed terms? If it is Lagrangian average, terms 2 and 3 on the right hand side of Eqs. 1 and 2 should be zero.

Response: The velocity and eddy viscosity have been decomposed into tidal averages and tidal oscillations utilizing the Eulerian mean method, for the following reasons:

Firstly, it is important to emphasize that the Eulerian mean method and the Lagrangian mean method are two mathematical approaches, both of which are inherently valid. However, they yield different types of residual currents—Eulerian residual currents and Lagrangian residual currents. To be considered as representations of residual flow fields, these currents must adhere to the characteristics of the flow field. As Lamb (1975) has indicated, any flow field must satisfy the principle of conservation of material surfaces. Eulerian residual currents do not adhere to the conservation of material surfaces, whereas Lagrangian residual currents do, which are suitable for describing long-term material transport.

Secondly, the momentum equation used in this study for physical oceanography is expressed in the Eulerian framework. The physical variables are obtained at each fixed location in the study domain. Initially described by Simpson et al. (1990), the process of tidal straining induces periodic stratification (SIPS), where tidal straining in the density field renders water columns unstable during flood tides and vice versa during ebb tides. This leads to enhanced small-scale turbulence and increased vertical mixing during flood tides, while vertical mixing is suppressed during ebb tides. Jay and Musiak (1994) demonstrated that this asymmetric mixing during the tidal cycle is the primary mechanism for generating residual currents. It is worth noting that the asymmetry in tidal mixing, as defined, is considered for each spatial point and is defined within the Eulerian framework. Therefore, in this study, we initially employed the Eulerian averaging method to obtain the four subcomponents of eddy viscosity components, which all meet momentum balance at each time and at each spatial point.

Thirdly, when investigating the dynamics of tidal straining-induced residual currents, earlier studies primarily applied Eulerian averaging method to all momentum terms, including tidal straining, in the momentum equation, resulting in the derivation

of tidal straining-induced Eulerian residual circulation (e.g., Burchard et al., 2011), later referred to as asymmetric turbulent mixing (ATM)-induced exchange flow (e.g., Cheng et al., 2011, 2013), and subsequently termed eddy viscosity–shear covariance (ESCO) flow (Dijkstra et al., 2017). In contrast, tidal straining-induced Lagrangian residual currents have not been extensively explored in previous research. Therefore, in this study, we applied Lagrangian averaging to all momentum terms, including tidal straining, in the momentum equation. The physical interpretation of this approach is that it considers the integrated effect of tidal straining at each point along the trajectory of particle motion.

Finally, when employing the Lagrangian averaging method to separate velocity and eddy viscosity into tidal averages and tidal oscillations, defining tidal asymmetry during flood and ebb tides poses a challenge. This is because particles pass through different spatial points at various times along their trajectory, rendering it challenging to establish a consistent concept of asymmetric tidal mixing that corresponds to previous definitions.

The tidal straining is represented by the ESCO, i.e. the eddy viscosity-shear covariance that is the tidal average of the product of tidal oscillations of velocity and eddy viscosity. Hence, tidal straining term is the fourth term rather than the second term in Eqs. 1 and 2.

Response: In the current manuscript, we express the horizontal velocities u and v as the sum of two components: $u=u_0+u_1$ and $v=v_0+v_1$, namely u_0 and v_0 representing the tidal periodic oscillation currents, "*which are referred to as the zero-order terms. These zero-order terms are equivalent in meaning to u' and v' as defined in prior studies (Burchard and Hetland, 2010; Burchard et al., 2011, 2014; Cheng, 2014). The terms* u_1 *and* v_1 *correspond to the first-order terms and represent the tidal average current*" (lines 211–214). Similarly, the eddy viscosity coefficient ν_h ($\nu_h = \nu_{h0} + \nu_{h1}$) is decomposed into ν_{h0}, representing the tidal average eddy viscosity "*as the zero-order term*", and "ν_{h1}, *representing the tidal periodic oscillation of the eddy viscosity as the first-order term*"(lines 214–216). Therefore, the third term in Eqs. (1) and (2) corresponds to the tidal straining circulation.

$$-\left\langle \frac{1}{D^2}\frac{\partial}{\partial\sigma}\left(\nu_h\frac{\partial u}{\partial\sigma}\right)\right\rangle /f = \underbrace{-\left\langle \frac{1}{D^2}\frac{\partial}{\partial\sigma}\left(\nu_{h0}\frac{\partial u_0}{\partial\sigma}\right)\right\rangle /f}_{1} \underbrace{-\left\langle \frac{1}{D^2}\frac{\partial}{\partial\sigma}\left(\nu_{h0}\frac{\partial u_1}{\partial\sigma}\right)\right\rangle /f}_{2} \underbrace{-\left\langle \frac{1}{D^2}\frac{\partial}{\partial\sigma}\left(\nu_{h1}\frac{\partial u_0}{\partial\sigma}\right)\right\rangle /f}_{3} \underbrace{-\left\langle \frac{1}{D^2}\frac{\partial}{\partial\sigma}\left(\nu_{h1}\frac{\partial u_1}{\partial\sigma}\right)\right\rangle /f}_{4}, \quad (1)$$

$$\left\langle \frac{1}{D^2}\frac{\partial}{\partial\sigma}\left(\nu_h\frac{\partial v}{\partial\sigma}\right)\right\rangle /f = \underbrace{\left\langle \frac{1}{D^2}\frac{\partial}{\partial\sigma}\left(\nu_{h0}\frac{\partial v_0}{\partial\sigma}\right)\right\rangle /f}_{1} + \underbrace{\left\langle \frac{1}{D^2}\frac{\partial}{\partial\sigma}\left(\nu_{h0}\frac{\partial v_1}{\partial\sigma}\right)\right\rangle /f}_{2} + \quad (2)$$

$$\underbrace{\left\langle \frac{1}{D^2}\frac{\partial}{\partial\sigma}\left(v_{h1}\frac{\partial v_0}{\partial\sigma}\right)\right\rangle/f}_{3}+\underbrace{\left\langle \frac{1}{D^2}\frac{\partial}{\partial\sigma}\left(v_{h1}\frac{\partial v_1}{\partial\sigma}\right)\right\rangle/f}_{4},$$

The detailed information (lines 226–232 in the revised manuscript) is as follows: "*The* $-\langle\frac{1}{D^2}\frac{\partial}{\partial\sigma}\left(v_{h0}\frac{\partial u_0}{\partial\sigma}\right)\rangle/f$ *and* $\langle\frac{1}{D^2}\frac{\partial}{\partial\sigma}\left(v_{h0}\frac{\partial v_0}{\partial\sigma}\right)\rangle/f$ *represent the coupled component of the tidal-average eddy viscosity and velocity gradient oscillation (*v_{Lk0u0} *and* u_{Lk0u0}*),* ***the*** $-\langle\frac{1}{D^2}\frac{\partial}{\partial\sigma}\left(v_{h1}\frac{\partial u_0}{\partial\sigma}\right)\rangle/f$ ***and*** $\langle\frac{1}{D^2}\frac{\partial}{\partial\sigma}\left(v_{h1}\frac{\partial v_0}{\partial\sigma}\right)\rangle/f$ ***represent the tidal straining component (*** v_{Lk1u0} ***and*** u_{Lk1u0}***),*** *the* $-\langle\frac{1}{D^2}\frac{\partial}{\partial\sigma}\left(v_{h0}\frac{\partial u_1}{\partial\sigma}\right)\rangle/f$ *and* $\langle\frac{1}{D^2}\frac{\partial}{\partial\sigma}\left(v_{h0}\frac{\partial v_1}{\partial\sigma}\right)\rangle/f$ *represent the turbulent mean component (*v_{Lk0u1} *and* u_{Lk0u1}*), the* $-\langle\frac{1}{D^2}\frac{\partial}{\partial\sigma}\left(v_{h1}\frac{\partial u_1}{\partial\sigma}\right)\rangle/f$ *and* $\langle\frac{1}{D^2}\frac{\partial}{\partial\sigma}\left(v_{h1}\frac{\partial v_1}{\partial\sigma}\right)\rangle/f$ *represent the coupled component of eddy viscosity oscillation and the tidal-average velocity gradient (*v_{Lk1u1} *and* u_{Lk1u1}*).* " The $-\langle\frac{1}{D^2}\frac{\partial}{\partial\sigma}\left(v_{h1}\frac{\partial u_0}{\partial\sigma}\right)\rangle/f$ and $\langle\frac{1}{D^2}\frac{\partial}{\partial\sigma}\left(v_{h1}\frac{\partial v_0}{\partial\sigma}\right)\rangle/f$ represent the tidal straining components of the LRV, corresponding to the third term in Eqs. (1) and (2). These components reflect the covariance between the oscillation of eddy viscosity and velocity shear, arising specifically due to the fact that v_{h1}, u_0, and v_0 are all oscillatory terms.

The relevant content has already been included in the revised manuscript (lines 211–226): "*which are referred to as the zero-order terms. These zero-order terms are equivalent in meaning to u' and v' as defined in prior studies (Burchard and Hetland, 2010; Burchard et al., 2011, 2014; Cheng, 2014). The terms* u_1 *and* v_1 *correspond to the first-order terms and represent the tidal average current*" "*as the zero-order term*", and "v_{h1}*, representing the tidal periodic oscillation of the eddy viscosity as the first-order term*".

The total water depth, D also changes with time, and needs to be decomposed in the same way as the velocity and eddy viscosity do.

Response: Applying a first-order Taylor expansion, the approximation of $1/D^2$ can be expressed as $1/H^2 - 2\zeta/H^3$ (Cheng, 2014), where H represents the mean depth, ζ denotes sea surface elevation. The four subcomponents of the eddy viscosity component, as delineated in Eqs. (1) and (2) in the revised manuscript, are further decomposed into eight distinct terms, detailed in Eqs. (A3) and (A4).

$$-\left\langle \frac{1}{D^2}\frac{\partial}{\partial\sigma}\left(v_h\frac{\partial u}{\partial\sigma}\right)\right\rangle/f=\underbrace{-\left\langle \frac{1}{H^2}\frac{\partial}{\partial\sigma}\left(v_{h0}\frac{\partial u_0}{\partial\sigma}\right)\right\rangle/f}_{1}\underbrace{-\left\langle \frac{1}{H^2}\frac{\partial}{\partial\sigma}\left(v_{h0}\frac{\partial u_1}{\partial\sigma}\right)\right\rangle/f}_{2}$$

$$\underbrace{-\left\langle\frac{1}{H^2}\frac{\partial}{\partial\sigma}\left(v_{h1}\frac{\partial u_0}{\partial\sigma}\right)\right\rangle/f}_{3}\underbrace{-\left\langle\frac{1}{H^2}\frac{\partial}{\partial\sigma}\left(v_{h1}\frac{\partial u_1}{\partial\sigma}\right)\right\rangle/f}_{4}$$

$$\underbrace{-\left\langle\frac{-2\zeta}{H^3}\frac{\partial}{\partial\sigma}\left(v_{h0}\frac{\partial u_0}{\partial\sigma}\right)\right\rangle/f}_{5}\underbrace{-\left\langle\frac{-2\zeta}{H^3}\frac{\partial}{\partial\sigma}\left(v_{h0}\frac{\partial u_1}{\partial\sigma}\right)\right\rangle/f}_{6}$$

$$\underbrace{-\left\langle\frac{-2\zeta}{H^3}\frac{\partial}{\partial\sigma}\left(v_{h1}\frac{\partial u_0}{\partial\sigma}\right)\right\rangle/f}_{7}\underbrace{-\left\langle\frac{-2\zeta}{H^3}\frac{\partial}{\partial\sigma}\left(v_{h1}\frac{\partial u_1}{\partial\sigma}\right)\right\rangle/f}_{8}, \tag{A3}$$

$$\left\langle\frac{1}{D^2}\frac{\partial}{\partial\sigma}\left(v_h\frac{\partial v}{\partial\sigma}\right)\right\rangle/f=\underbrace{\left\langle\frac{1}{H^2}\frac{\partial}{\partial\sigma}\left(v_{h0}\frac{\partial v_0}{\partial\sigma}\right)\right\rangle/f}_{1}+\underbrace{\left\langle\frac{1}{H^2}\frac{\partial}{\partial\sigma}\left(v_{h0}\frac{\partial v_1}{\partial\sigma}\right)\right\rangle/f}_{2}+$$

$$\underbrace{\left\langle\frac{1}{H^2}\frac{\partial}{\partial\sigma}\left(v_{h1}\frac{\partial v_0}{\partial\sigma}\right)\right\rangle/f}_{3}+\underbrace{\left\langle\frac{1}{H^2}\frac{\partial}{\partial\sigma}\left(v_{h1}\frac{\partial v_1}{\partial\sigma}\right)\right\rangle/f}_{4}+$$

$$\underbrace{\left\langle\frac{-2\zeta}{H^3}\frac{\partial}{\partial\sigma}\left(v_{h0}\frac{\partial v_0}{\partial\sigma}\right)\right\rangle/f}_{5}+\underbrace{\left\langle\frac{-2\zeta}{H^3}\frac{\partial}{\partial\sigma}\left(v_{h0}\frac{\partial v_1}{\partial\sigma}\right)\right\rangle/f}_{6}+$$

$$\underbrace{\left\langle\frac{-2\zeta}{H^3}\frac{\partial}{\partial\sigma}\left(v_{h1}\frac{\partial v_0}{\partial\sigma}\right)\right\rangle/f}_{7}+\underbrace{\left\langle\frac{-2\zeta}{H^3}\frac{\partial}{\partial\sigma}\left(v_{h1}\frac{\partial v_1}{\partial\sigma}\right)\right\rangle/f}_{8}, \tag{A4}$$

In the majority of the Pearl River Estuary, the ratio of maximum sea surface elevation (ζ_{max}) to mean water depth (H) is less than 0.2 during neap tides, except in the nearshore areas. The terms related to $-2\zeta/H^3$, including the fifth to eighth terms in Eqs. (A3) and (A4), are so minimal that they can be considered negligible during neap tides (Fig. A2a3–j3). Conversely, the terms related to $1/H^2$, comprising the first to fourth terms (Fig. A2a2–j2) in Eqs. (A3) and (A4), demonstrate a notable congruence with the terms related to$1/D^2$ in structure and magnitude during neap tides (Fig. A2a1–j1). During spring tides, although the ratio of ζ_{max} to H is slightly larger than those during neap tides, the terms associated with $1/H^2$ (Fig. A3a2–j2) continue to predominate in both structure and magnitude over the components related to $1/D^2$ (Fig. A3a1–j1). Additionally, while the terms associated with $-2\zeta/H^3$ (Fig. A3a3–j3) are greater during spring tides than during neap tides, their contribution to the total components remains significantly less than those related to $1/H^2$. Given that D is approximately equal to H, D is not decomposed further in the manuscript. The relevant content has already been included in the revised manuscript (lines 217–226). "*Employing a first-order Taylor expansion, the approximation of $1/D^2$ is represented as $1/H^2–2\zeta/H^3$ (Cheng, 2014), where H signifies the mean depth and ζ corresponds to the sea surface elevation. Within the vast majority of the Pearl River Estuary, the ratio of ζ_{max} to H remains below 0.2 during neap tides, with an exception in nearshore areas, where ζ_{max} is the maximum of*

tidal elevations during a tidal period. The ratio during spring tides is slightly bigger than that during neap tides. But whether during spring or neap tides, the terms associated with $1/H^2$ *exhibit a close correspondence to those related to* $1/D^2$ *in Eqs. (1) and (2) (not shown). The terms pertaining to* $-2\zeta/H^3$ *are sufficiently minor to be negligible. Consequently, considering D is approximately equivalent to H, further decomposition of D in the manuscript is not undertaken*."

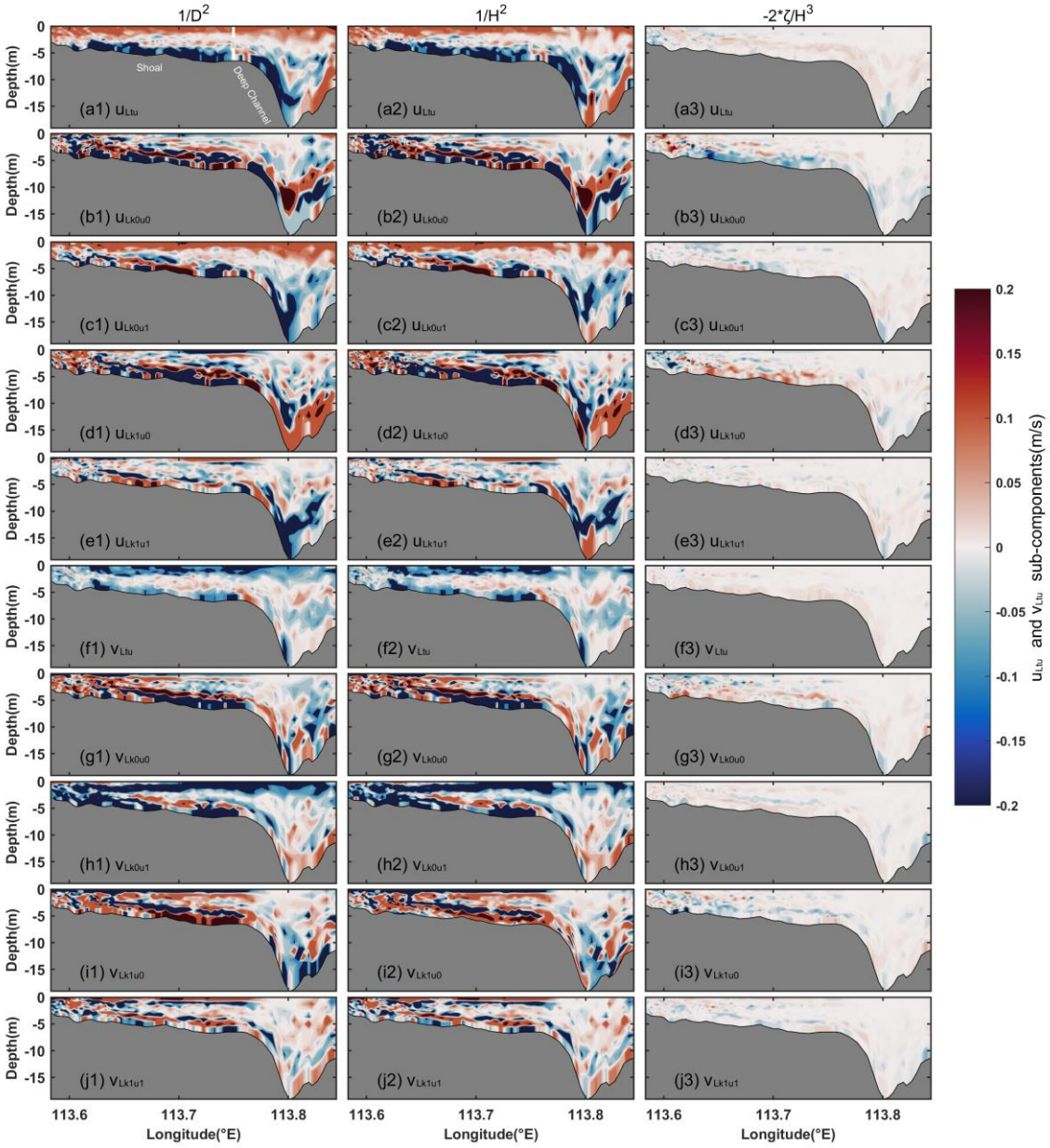

Figure A2 Vertical profiles of each subcomponent of the eddy viscosity during neap tides. **(a1–j1)** terms related to $1/D^2$, **(a2–j2)** terms related to $1/H^2$, **(a3–j3)** terms related to $-2\zeta/H^3$. For cross-estuary direction: **(a1, a2, a3)** total eddy viscosity component related to $1/D^2$, $1/H^2$ and $-2\zeta/H^3$, respectively; **(b1, b2, b3)** coupled component of the tidal-average eddy viscosity and velocity gradient oscillation (u_{Lk0u0}) related to $1/D^2$, $1/H^2$ and $-2\zeta/H^3$; **(c1, c2, c3)** turbulent mean component (u_{Lk0u1}) related to $1/D^2$, $1/H^2$ and $-2\zeta/H^3$, **(d1, d2, d3)** tidal straining component (u_{Lk1u0}) related to $1/D^2$, $1/H^2$ and $-2\zeta/H^3$; **(e1, e2, e3)** coupled component of eddy viscosity oscillation and the tidal-average velocity gradient (u_{Lk1u1}) related to $1/D^2$, $1/H^2$ and $-2\zeta/H^3$, respectively. **(f1–j1; f2–j2; f3–j3)** Corresponding along-estuary subcomponents related to $1/D^2$, $1/H^2$ and $-2\zeta/H^3$.

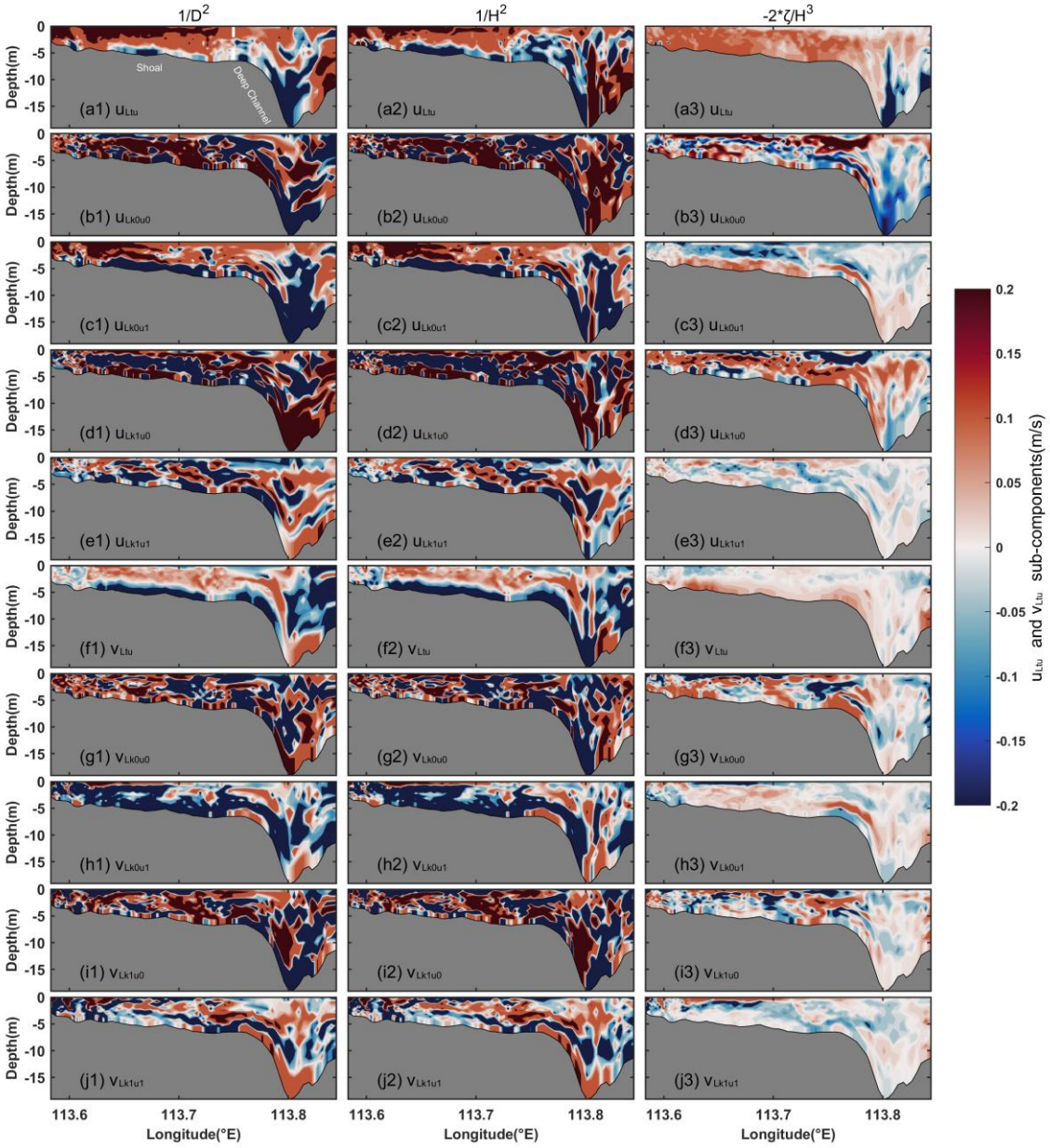

Figure A3 Same as Fig. A2, but for spring tides.

Fig. 4 b, line 280-282. Why does the barotropic component have a vertical two-layer structure?

Response: To elucidate the two-layer structure of the barotropic component of LRV as depicted in Fig. A4a, we conducted an integration of the barotropic pressure gradient forcing (BPG) along the particle's trajectory throughout a tidal cycle, denominated as Lagrangian integrated BPG. This methodology encompasses the cumulative effects at each point traversed by the particle. Distinct trajectories undertaken by surface and bottom particles result in divergent outcomes with different magnitudes and opposing signs for the Lagrangian integrated BPG across the upper and lower layers, as illustrated in Fig. A4b–c. The Lagrangian integrated BPG at the final step, divided by one tidal period, yields the Lagrangian mean BPG. Consequently, the corresponding Lagrangian

residual velocity is characterized by a vertically sheared two-layer structure with opposite flow directions. Contrastingly, the Eulerian mean BPG, averaged at fixed spatial points, exhibits a homogeneous vertical profile (Fig. A5a). Notably, discrepancies are also observed between Lagrangian integrated and Eulerian mean baroclinic pressure gradient forcings, expounded upon in Fig. A4d–f and Fig. A5b. The related explanation has been added in the manuscript (lines 341–344). "*The two-layer structure of u_{Lba} arises from the distinct trajectories of particles in the upper and lower layers. The integration results along these different trajectories produce varying magnitudes and opposite directions of u_{Lba} components in both layers.*"

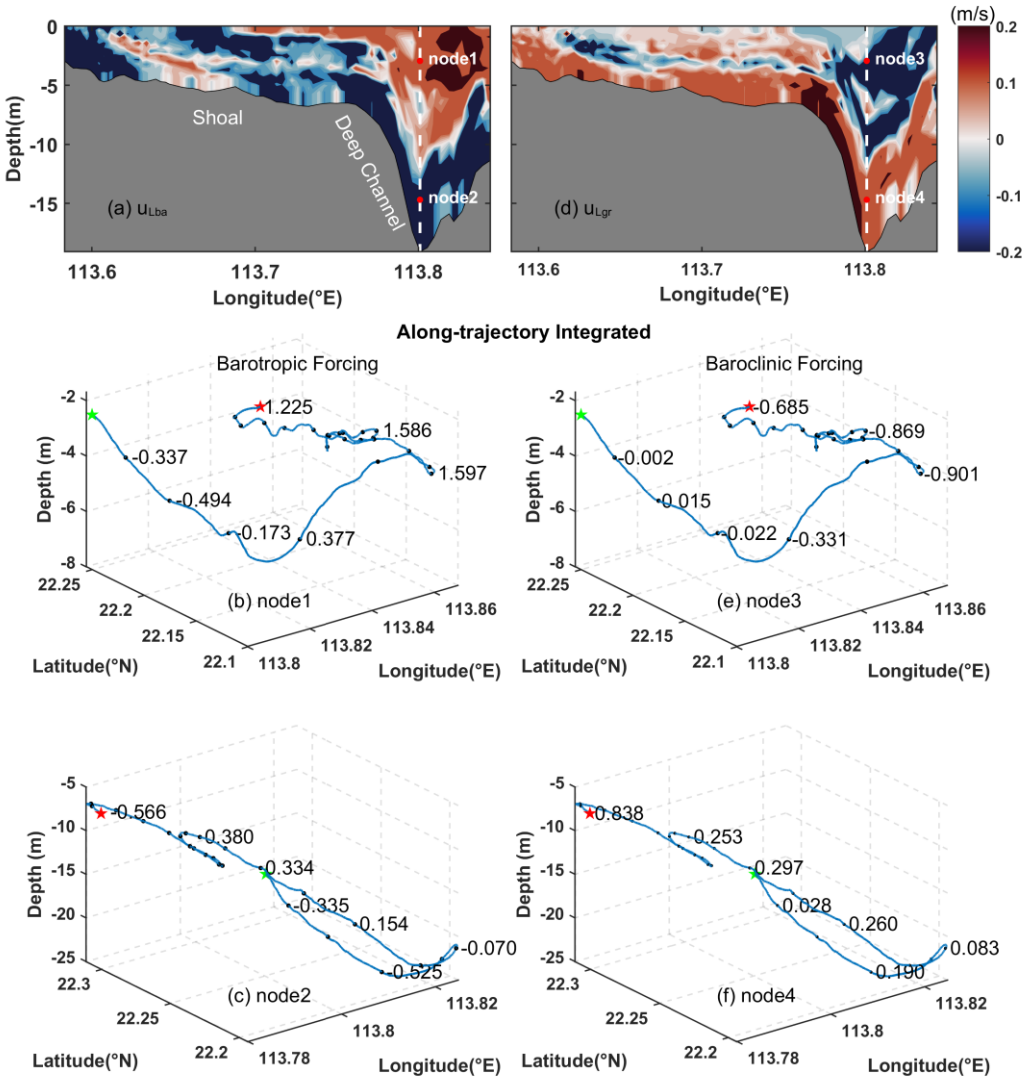

Figure A4 (a) The cross-estuary barotropic component of the Lagrangian Residual Velocity (LRV), with two red nodes (nodes 1 and 2) in the deep channel indicating locations of eastward and westward flow, respectively. **(b, c)** Lagrangian-integrated barotropic pressure gradient along the trajectories of particles at nodes 1 and 2, respectively. The green star marks the starting location, while the red star denotes the ending location. The particle trajectories are traced with blue lines. **(d–f)** Same as **(a–c)**, but for the baroclinic component of LRV at nodes 3 and 4, respectively.

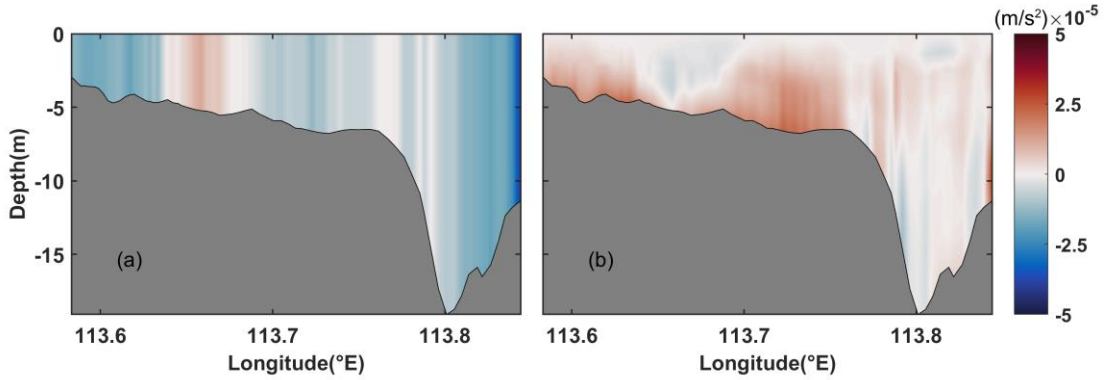

Figure A5 Vertical profiles of the Eulerian mean **(a)** barotropic and **(b)** baroclinic pressure gradient forcing in Section C.

Reference

Burchard, H., Hetland, R. D.: Quantifying the contributions of tidal straining and gravitational circulation to residual circulation in periodically stratified tidal estuaries, J. Phys. Oceanogr., 40(6), 1243–1262, https://doi.org/10.1175/2010JPO4270.1, 2010.

Burchard, H., Hetland, R. D., Schulz, E., Schuttelaars, H. M.: Drivers of residual estuarine circulation in tidally energetic estuaries: Straight and irrotational channels with parabolic cross section, J. Phys. Oceanogr., 41(3), 548–570, https://doi.org/10.1175/2010JPO4453.1, 2011.

Burchard, H., Schulz, E., Schuttelaars, H. M.: Impact of estuarine convergence on residual circulation in tidally energetic estuaries and inlets, Geophys. Res. Lett., 41(3), 913–919, https://doi. org/10.1002/2013GL058494, 2014.

Chen, Y., Cui, Y. X., Sheng, X. X., Jiang, W. S., Feng, S. Z.: Analytical solution to the 3D tide-induced Lagrangian residual current in a narrow bay with vertically varying eddy viscosity coefficient, Ocean Dyn., 70, 759–770, https://doi.org/10.1007/s10236-020-01359-3, 2020.

Chen, Y. R., Chen, L. H., Zhang, H., Gong, W. P.: Effects of wave-current interaction on the Pearl River Estuary during Typhoon Hato, Estuar. Coast. Shelf Sci., 228, 106364, https://doi.org/10.1016/j.ecss.2019.106364, 2019.

Cheng, P.: Decomposition of residual circulation in estuaries, J. Atmos. Ocean. Tech., 31(3), 698–713, 2014.

Cheng, P., de Swart H. E., Valle-Levinson, A.: Role of asymmetric tidal mixing in the subtidal dynamics of narrow estuaries, J. Geophys. Res.: Oceans, 118(5), 2623–2639, https://doi.org/10.1002/jgrc.20189, 2013.

Cheng, P., Valle-Levinson, A., de Swart, H. E.: A numerical study of residual circulation induced by asymmetric tidal mixing in tidally dominated estuaries, J. Geophys. Res.: Oceans, 116(C1), https://doi.org/10.1029/2010JC006137, 2011.

Cui, Y. X., Jiang, W. S., Deng, F. J.: 3D numerical computation of the tidally induced Lagrangian residual current in an idealized bay, Ocean Dyn., 69, 283–300, https://doi.org/10.1007/s10236-018-01243-1, 2019.

Dijkstra, Y. M., Schuttelaars, H. M., Burchard, H.: Generation of exchange flows in estuaries by tidal and gravitational eddy viscosity-shear covariance (ESCO), J. Geophys. Res.: Oceans, 122(5), 4217–4237, https://doi.org/10.1002/2016JC012379, 2017.

Jay, D. A., Musiak, J. D.: Particle trapping in estuarine tidal flows, J. Geophys. Res.: Oceans, 99(C10), 20445–20461, https://doi.org/10.1029/94JC00971, 1994.

Jiang, W. S., Feng, S. Z.: Analytical solution for the tidally induced Lagrangian residual current in a narrow bay, Ocean Dyn., 61, 543–558, https://doi.org/10.1007/s10236-011-0381-z, 2011.

Jiang, W. S., Feng, S. Z.: 3D analytical solution to the tidally induced Lagrangian residual current equations in a narrow bay, Ocean Dyn., 64, 1073–1091, https://doi.org/10.1007/s10236-014-0738-1, 2014.

Lai, W. F., Pan, J. Y., Devlin, A. T.: Impact of tides and winds on estuarine circulation in the Pearl River Estuary, Cont. Shelf Res., 168, 68–82, https://doi.org/10.1016/j.csr.2018.09.004, 2018.

Lamb, H.: Hydrodynamics, London: Cambridge university press, 1975.

Li, M. Q., Wang, N., Li, G. X., Song, D. H., Gu, Y. Z., Bao, X. W., Liu, S. D., Zhang, L.: Plume bulge observed in the Pearl River Estuary in summer: Spatiotemporal characteristics and influencing factors, Estuar. Coast. Shelf Sci., 282, 108242, 2023.

Pan, J. Y., Gu, Y. Z., Wang, D. X.: Observations and numerical modeling of the Pearl River plume in summer season, J. Geophys. Res.: Oceans, 119(4), 2480–2500, 2014.

Simpson, J. H., Brown, J., Matthews, J., Allen, G.: Tidal straining, density currents, and stirring in the control of estuarine stratification, Estuaries 13, 125–132, https://doi.org/10.2307/1351581, 1990.

Wu, H., Gu, J. H., Zhu, P.: Winter counter-wind transport in the inner southwestern Yellow Sea, J. Geophys. Res.: Oceans, 123(1), 411–436, 2018.